Available online at www.sciencedirect.com

ScienceDirect

journal homepage: www.elsevier.com/locate/issn/15375110

Research Paper

Investigation into the vibration characteristics of agricultural wheeled tractor-implement system with hydro-pneumatic suspension on the front axle

Enlai Zheng [a,*], *Xinyu Zhong* [a], *Rui Zhu* [b], *Jinlin Xue* [a], *Song Cui* [a], *Huisong Gao* [a], *Xiangze Lin* [a]

[a] *Department of Mechanical Engineering, College of Engineering, Nanjing Agricultural University, Nanjing, 210031, China*

[b] *School of Mechanical Engineering, Southeast University, Nanjing, 211189, China*

ARTICLE INFO

Article history:
Received 12 November 2018
Received in revised form
29 March 2019
Accepted 17 May 2019
Published online 10 July 2019

Keywords:
Wheeled tractor
Hydro-pneumatic suspension
Vibration
Implement

Before predicting the vibration characteristics of a tractor/implement system with front axle hydro-pneumatic suspension, it is essential to develop a dynamic model. The nonlinear stiffness and damping calculation equations for hydro-pneumatic suspension are derived and the complete three dimensional multibody dynamic model of the wheeled tractor/implement system is presented in this paper. The construction of the model considers the effect of implement and passive rub cabin suspension as well as front axle hydro-pneumatic suspension together. The vibration responses and the corresponding power spectral densities (PSD) of driver seat, cabin, chassis and implement under different forward speed and field road conditions gathered from the simulation using the models are in good agreement with experimental results, demonstrating the effectiveness of the proposed model. A comparative investigation on the dynamic effects of a passive cabin suspension, implement and front axle hydro-pneumatic suspension under four cases was made. The effects of front axle suspension and the implement on the rollover limit chart for the tractor system were also studied. Simulation results showed that the front axle hydro-pneumatic suspension will deteriorate the ride comfort of drivers but will improve pitch and roll stability. Passive cabin suspension plays a more important role in improving the ride comfort of drivers than the front axle hydro-pneumatic suspension does, while compromising the pitch stability to some extent. The implement will raise the riding comfort of drivers and the pitch stability of tractors, but dramatically worsen the roll stability. The presence of the front axle suspension and the implement improves the minimum slope angle and reduces the maximum slope angle. Furthermore, the effect of the initial nitrogen volume, the pressure of energy accumulators, and the orifice diameter of the small throttle valves on the vibration characteristics of the tractor system with the large throttle valve closed or fully opened is also investigated.

© 2019 IAgrE. Published by Elsevier Ltd. All rights reserved.

* *Corresponding author*. Department of Mechanical Engineering, College of Engineering, Nanjing Agricultural University, 40 DianJiangTai Road, Pukou District, Nanjing, 210031, China. Fax: +025 58606699.
E-mail address: enlaizheng@njau.edu.cn (E. Zheng).

https://doi.org/10.1016/j.biosystemseng.2019.05.004

1537-5110/© 2019 IAgrE. Published by Elsevier Ltd. All rights reserved.

Nomenclature

$k_{tx,fl}, k_{tx,fr}, k_{tx,rl}, k_{tx,rr}$	Longitudinal stiffness of front and rear tyres, N m^{-1}
$k_{ty,fl}, k_{ty,fr}, k_{ty,rl}, k_{ty,rr}$	Lateral stiffness of front and rear tyres, N m^{-1}
$k_{tz,fl}, k_{tz,fr}, k_{tz,rl}, k_{tz,rr}$	Vertical stiffness of front and rear tyres, N m^{-1}
$c_{tx,fl}, c_{tx,fr}, c_{tx,rl}, c_{tx,rr}$	Longitudinal damping of front and rear tyres, N s m^{-1}
$c_{ty,fl}, c_{ty,fr}, c_{ty,rl}, c_{ty,rr}$	Lateral damping of front and rear tyres, N s m^{-1}
$c_{tz,fl}, c_{tz,fr}, c_{tz,rl}, c_{tz,rr}$	Vertical damping of front and rear tyres, N s m^{-1}
$k_{cfl}, k_{cfr}, k_{crl}, k_{crr}$	Vertical stiffness of cabin, N m^{-1}
$c_{cfl}, c_{cfr}, c_{crl}, c_{crr}$	Vertical damping of cabin, N s m^{-1}
k_d, c_d	Stiffness and damping of driver seat, N m^{-1}, N s m^{-1}
k_{sfl}, k_{sfr}	Vertical stiffness of front axle suspension, N m^{-1}
$\varphi_{b1}\varphi_{b2}, \varphi_{b3}$	Pitch, roll and yaw angle of chassis around the y, x and z axles, rad
$\varphi_{c1}, \varphi_{c2}$	Pitch and roll angle of cabin around y and x axles, rad
φ_f	Roll angel of front axle around the x axis, rad
m_a, m_b, m_c, m_d, m_f	Mass of implement, chassis, cabin, driver and front axle, kg
m_e	Equivalent mass of chassis and implement, kg
$J_{b1}J_{b2}J_{b3}$	Pitch, roll and yaw moment of inertia for chassis around the y, x and z axles, kg m^2
$J_{c1}J_{c2}$	Pitch and roll moment of inertia for cabin around the y and x axles, kg m^2
J_f	Roll moment of inertia for front axle around the x axis, kg m^2
z_b, z_c, z_d, z_f	Vertical displacement of mass centre for chassis, cabin, driver and front axle, m
x_b, y_b	Longitudinal and lateral displacement of chassis, m
q_f, q_r	Excitations of front and rear axles due to road roughness, m
l_f, l_r	Distance between front axle and mass centre of chassis, rear axle and mass centre of chassis, m
l_{bf}, l_{br}	Distance between the front cabin suspension and mass centre of chassis, the rear cabin suspension and mass centre of chassis, m
$\ddot{\varphi}_{b1}, \ddot{\varphi}_{b2}$	Pitch and roll vibration acceleration of chassis around the y, x and z axles, rad s^{-2}
$\ddot{x}_b, \ddot{y}_b, \ddot{z}_b$	Longitudinal, lateral and vertical vibration acceleration of chassis, m s^{-2}
F_{fdyn}	Dynamic load of two front tyres, N
l_{sw}, l_{bw}	Distance between front axle suspension and gravity centre of chassis, between front tyre and gravity centre of chassis, m
l_{cf}, l_{cr}	Distance between the front cabin suspension and mass centre of cabin, the rear cabin suspension and mass centre of cabin, m
l_d	Distance between the driver seat and mass centre of cabin, m
r_f, r_r	Radius of front and rear tyres, m
σ	Orientation of the tractor on the slope, rad
β	Angle of slope, rad
p	Distance between front and rear axles, $p = l_f + l_r$, m
t_{fl}, t_{fr}	Half of the front track for two rear tyres, m
t_{rl}, t_{rr}	Half of the front track for two rear tyres, m
h_p	Distance between upper end of piston rod and road, m
h_f, h_r	Height of front and rear roll centres, m
h_g	Height of gravity centre, m
h_0	Height of the roll axle at the gravity centre, m
y_g	Lateral displacement of gravity centre, m
k_f, k_r	Vertical stiffness of front and rear tyres, N m^{-1}
r_f, r_r	Radius of front and rear tyres, m
ρ_r	Roll angle at the front axle, rad

1. Introduction

The low-frequency vibration experienced by an agricultural tractor comes from the interaction between the tractor and the rough terrain (Muzammil, Siddiqui, & Hasan, 2004; Prasad, Tewari, & Yadav, 1995; Scarlett, Price, & Stayner, 2007). The vibration will be severe when the tyres are the only elastic component between road and tractor body. Tyres are unable to provide proper suspension functions of absorbing these oscillations, excessive exposure to these vibrations may cause discomfort and even result in health problems, hindering performance and increasing the risk of accidents. Moreover, tractor vibration leads to increased tyre dynamic load, which will not only destroy the road and compact the farmland soil (Arvidsson & Ristic, 1996; Hildebrand, Keskinen, & Navarrete, 2008; Kumar, Mahajan, Mohan, & Varghese, 2001; Lines, Stiles, & Whyte, 1995; Marsili, Ragni, Santoro, Servadio, & Vassalini, 2002), but also affect the handling stability and the safety of the tractor. With the development of technology, the front axle of modern tractors have been equipped with hydro-pneumatic suspension. Therefore, it's essential to develop a dynamic model of tractor/implement system with front axle suspension. Based on the model, the vibration characteristics and performance can be evaluated, providing a theoretical basis for the structural design and parameter optimisation of the suspension and tractor system.

The main feature of this study is that it considers the hydro-pneumatic suspension on the front axle, the three-point hitch structure between implement and tractor frame, the excitations from road surface roughness, which leads to strong nonlinear vibrations. There are six degree of freedom (DOFs) relevant with the tractor body motions including three translational and three rotational DOFs. Thus, it's challenging to build an integrated dynamic model of wheeled tractor/implement system with hydro-pneumatic suspension on front axle involved.

The methods of investigating the vibration characteristics of agricultural tractors distinguish two main categories: experimental methods (Clijmans, Ramon, & De Baerdemaeker, 1998; Cuong, Zhu, & Zhu, 2013; Nguyen & Inaba, 2011; Zehsaz, Sadeghi, Ettefagh, & Shams, 2011; Cutini, Costa, & Bisaglia, 2016; Adam & Jalil, 2017) and computer simulation methods. Although experimental methods can provide results with high precision and good reliability, the high cost, insecurity and inconvenience limit their application. Moreover, experimental results rely highly on the type of the test tractor and the field conditions, which also restricts the promotion of experimental methods (Yang, Ren, Chen, Jiang, & Yang, 2009).

Computer simulation method employs the mathematical models or multibody dynamic models constructed by commercial software (Lehtonen & Juhala, 2005; Shahgoli, Fielke, Saunders, & Desbiolles, 2010) to extrapolate the experimental results over the range of test conditions. The quarter-vehicle model, half-vehicle model and full-vehicle body models have been developed to predict the dynamic behaviour of tractors and perform vibration control. The one-dimensional quarter-vehicle models with single or two DOFs are commonly used to study the heave motion of the tractor body (Cuong, Zhu, & Ngoc, 2014; Hammond & Harrison, 1981; Yuan et al., 2017). The half-vehicle is a two-dimensional model, generally representing the tractor's longitudinal dynamics and pitch motion of the tractor body as well as the vertical motion of the front and rear wheels (Gobbi, Mastinu, & Previati, 2014; Rehnberg, 2011; Zehsaz et al., 2011; Zheng, Fan, Zhu, Zhu, & Xian, 2016; Zhu et al, 1999, 2014). It can also be used to describe the lateral dynamics, the roll and heave motion of the tractor body and vertical motion of the left and right wheels. The number of DOFs of the three-dimensional full-tractor model ranges from six up to hundreds (Li, Mitsuoka, Inoue, Okayasu, & Hirai, 2015; Melzi, Negrini, & Sabbioni, 2014; Rabbani, Tsujimoto, Mitsuoka, Inoue, & Okayasu, 2011; Sim, Lee, Yoon, Choi, & Hwang, 2017). The specific number depends on the amount of components being modelled, the model versatility, and the simplifying assumptions being used.

In addition to the cabin and driver seat suspension (Ahmed & Goupillon, 1997; De Temmerman, Deprez, Anthonis, & Ramon, 2004; Deprez, Moshou, Anthonis, Baerdemaeker, & Ramon, 2005), for the sake of improving the driver's comfort and steering reliability, front axle suspension has always been the focus of this research. To the tractor without implement, the front axle elastic suspension had limited effect on the vertical vibration and driving safety depending on the driving conditions (Martelli, Paoluzzi, & Zarotti, 2002), while its effect on the pitch and lateral vibration is obvious (Gobbi et al., 2014). When the implement is mounted in front of a tractor, the effect of the front axle elastic suspension relies on the damping element, but it was less effective than that without front implement (Mazhei, Uspenskiy, & Ermalenok, 2006). Apart from the linear elastic front axle suspension, the hydro-pneumatic nonlinear suspension is also designed as the front axle suspension of tractor (Mazhei et al., 2006). To predict the output force of hydro-pneumatic suspension, its mathematical model is developed (Theron & Els, 2007; van der Westhuizen & Els, 2015; Yin, Rakheja, Yang, & Boileau, 2018) and the validity of the model is proved by experimental rig in the laboratory. Unlike the conventional linear elastic front axle suspension, the hydro-pneumatic nonlinear suspension plays an important role in reducing the vertical vibration acceleration and pitching vibration angular acceleration of the tractor (Yilidaer, Zhu, Xu, & Yuan, 2015).

It appears that no attempts have been made to study the effect of front axle hydro-pneumatic suspension and passive cabin suspension on the vibration characteristics of agricultural tractor/implement system involving the structure of three points hitch. In this work, three dimensional multibody dynamic model of wheeled tractor/implement system including hydro-pneumatic suspension on front axle is established, the corresponding vibration characteristics are analysed. Furthermore, the effects of the forward speed, the field road condition, the nitrogen volume, the pressure of accumulators, the orifice area of proportional and throttle valves is also studied.

This paper is organised as follows: The physical structure of the wheeled tractor/implement system including both the hydro-pneumatic suspension of front axle and the passive rubber suspension of cabin is introduced in section 2. The three dimensional multibody dynamic model of wheeled tractor/implement system including front axle hydro-pneumatic suspension is developed and parameters of tractor system are determined in section 3. Numerical simulation of vibration performances of wheeled tractor/implement system including front axle hydro-pneumatic suspension are conducted and discussed in section 4. The proposed dynamic model of wheeled tractor/implement system including front axle hydro-pneumatic suspension is summarised, the corresponding conclusions and recommendations for further research are presented in section 5.

2. Structure description

The installation diagram of the front axle hydro-pneumatic suspension system for the wheeled tractor/implement system in this work is shown in Fig. 1. The upper end of the piston rod and the lower end of the oil cylinder in the front axle hydro-pneumatic suspension system are hinged with chassis and front axle, respectively. The thrust bars between the front axle and chassis are used to support part of the longitudinal and transverse forces, while the guide bars are applied to restrict the relative movement of the front axle. To simplify the model, the effect of thrust and guide bars on the vibration characteristics of agricultural wheeled tractor-implement system is neglected.

The overall structure of the front axle hydro-pneumatic suspension system is composed of two parts: a hydro-pneumatic suspension system and a horizontal position adjustment system, as shown in Fig. 2 The hydro-pneumatic suspension for front axle is mainly composed of a rodless cavity (1), rod cavity (2), piston rod (3), piston (4), proportional valves (5, 7), small throttle valves (6, 8), large throttle valves (9, 10), and accumulators (A, B, C). The rodless cavity 1 is connected with accumulator A through the proportional valve 5 and small throttle valve 6 in series. Similarly, the rod cavity 2 is connected with accumulator B through

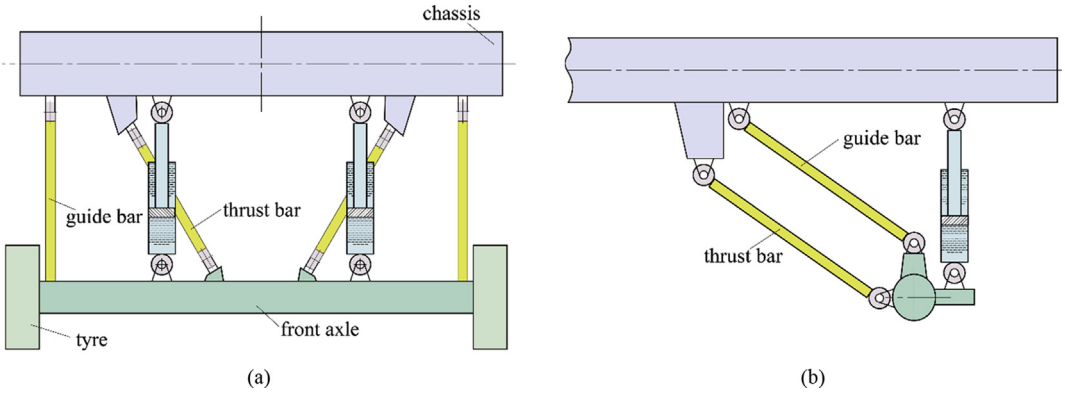


Fig. 1 – Installation diagram of front axle hydro-pneumatic suspension: (a) front view, (b) right view.

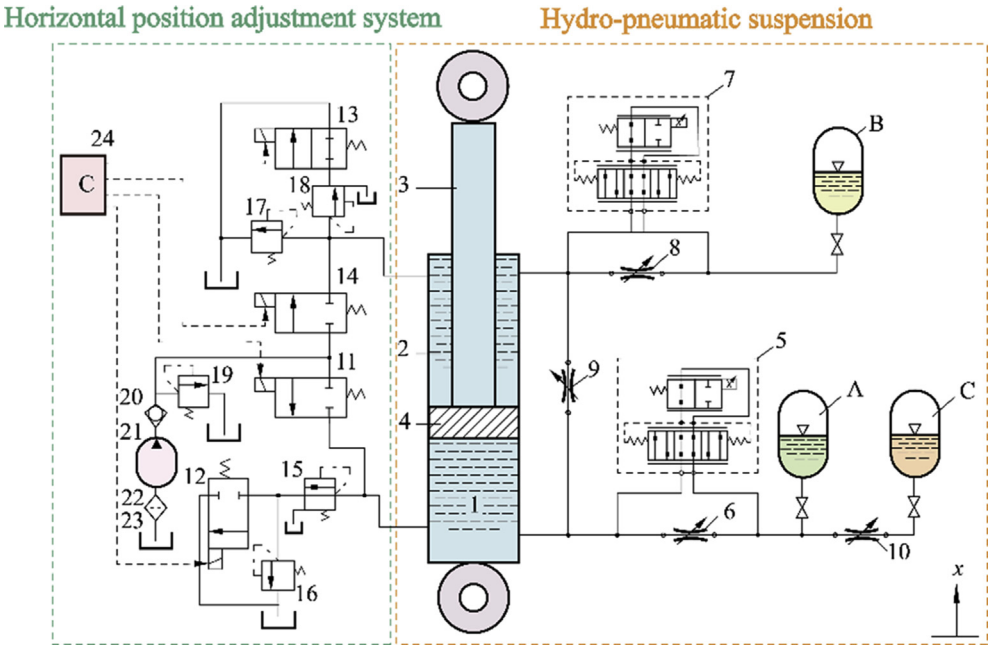


Fig. 2 – Overall structure of front axle hydro-pneumatic suspension system.

proportional valve 7 and small throttle valve 8 in series. To control the oil pressure between rod cavity 2 and rodless cavity 1, the accumulator A is linked with accumulator C through large throttle valve 10, the oil cylinders in accumulators A, B and C are separated from the nitrogen chamber using the membrane.

The piston rod and oil cylinder of the hydro-pneumatic suspension are hinged with front axle and chassis, respectively. When the wheeled tractor system travels on the uneven road, the relative motion between the front axle and the chassis enables the piston rod to reciprocate along the oil cylinder. When the front axle approaches the chassis and the throttle valve 9 is closed, the hydro-pneumatic suspension is compressed and the volume of rodless cavity reduces. The oil pressure in the rodless cavity 1 increases, the oil flows to accumulator A through proportional valve 5 and small throttle valve 6. In contrast, the oil pressure in the rod cavity 2 reduces, the oil in the accumulator B flows to the rod cavity 2 through proportional valve 7 and small throttle valve 8 until the pressure reaches equilibrium. In similar, when the front axle is separated from the chassis, the whole oil flow direction is opposite to that above. If the throttle valve 9 is opened, not only the oil in the oil cylinder flows mutually to accumulators, but some oil in the rodless and rod cavity will flow mutually whether the hydro-pneumatic suspension is compressed or not.

When the solenoid valves 11–14 are opened, the horizontal position adjustment system does not operate. The oil in the tank 23 enters into the hydraulic pump 21 through the strainer 22, which makes the check valve 20 work. Then, as all of the solenoid valves are in the closed state, the oil will return to the oil tank through the overflow valve 19. Each

solenoid valve is controlled by controller 24 to ensure whether solenoid valves 11 and 13, 12 and 14 are energised (or not) at the same time. Solenoid valves 11 and 14 cannot be energised at the same time. The power state of the controller 24 is determined by the state of displacement sensor mounted on the front axle. When the electromagnetic valves 11 and 13 are opened, the oil flows through the hydraulic pump 21 and the check valve 20 into rodless cavity 1. Then, the pressure and the volume of the rodless cavity 1 increase, which leads to the upward movement of piston 4, the reduction of volume and the increase of pressure of the rod cavity 2. After reaching a certain level of pressure, the sequence valve 18 will open and the oil will flow back to the tank through the electromagnetic valve 13. Then, the piston rod 3 moves upward until it reaches the required position. The solenoid valves 11 and 13 are closed to keep the position of the piston rod. Similarly, when the solenoid valves 12 and 14 are open, the oil from the hydraulic pump 21 will flow into the rod cavity 2 through the check valve 20 and the electromagnetic valve 14, meanwhile the pressure and the volume of rod cavity 2 will also increase, which drives the piston 4 to move downward. Then, the volume of the rodless cavity 1 reduces and its pressure rises. After reaching a certain level of pressure, the oil flows back to tank through the sequence valve 15 and the electromagnetic valve 12. At this point, the piston rod 3 moves downward until it reaches the required position. The horizontal position of the tractor body can be adjusted by controlling the power of the solenoid valves in the system. When the road surface is poor, the length of hydro-pneumatic suspension on both sides can be stretched to increase the height of gravity centre for tractor system. When the tractor runs on the flat road, the length of hydro-pneumatic suspension on both sides can be reduced. If the tractor system transports on a road with a transverse inclination, the hydraulic cylinders on one side can be extended and that on the other side can be shortened to maintain the horizontal posture of the tractor body.

The implement is connected with the tractor's body using the three-point hitch structure shown in Fig. 3(a) and the three-point hitch structure mainly comprises the lift shaft, lift arm, upper link, lift link, lower link and plough mounting bracket. When the lift shaft rotates, the plough mounting bracket will get off the ground through lift and upper links. Furthermore, to improve the ride comfort of tractor operators, a passive rubber suspension is installed between the cabin and the chassis, as shown in Fig. 3(b).

3. Dynamic model of wheeled tractor/implement with front axle hydro-pneumatic suspension

It is assumed that the cabin and the driver seat are rigidly connected with the chassis in the longitudinal and lateral directions. The effect of stiffness of the thrust and the guide bars is not considered in this work to simplify the model. The multibody dynamic model of the wheeled tractor/implement system with hydro-pneumatic suspension on front axle is developed, as shown in Fig. 4. The tractor is subjected to the displacement excitations $q_f(t)$ and $q_r(t)$ respectively at the front and rear tyres. Since there is a difference between amplitudes $q_f(t)$ and $q_r(t)$, the angular displacement subjected to the mass centre arises.

The road excitations relation between the front and the rear axles of the tractor at instant i by considering the time lag τ between $q_{fi}(t)$ and $q_{ri}(t)$ can be expressed as:

$$q_{f_i}(t) = q_{ri}(t+\tau) \tag{1}$$

where $q_{f_i}(t)$ and $q_{ri}(t)$ are displacement excitations at the front and the rear axles respectively, τ is the time lag and can be calculated by $(l_{bf} + l_{br})/v$, l_{bf} is the distance between the mass centre of chassis and that of the front axle, l_{br} is the distance between the mass centre of the chassis and that of the rear axle, v is the velocity of the tractor.

The generalised coordinates vectors for the multibody dynamic model of the tractor/implement system are defined as:

$$\mathbf{q} = \begin{bmatrix} z_b & \varphi_{b1} & \varphi_{b2} & z_c & \varphi_{c1} & \varphi_{c2} & z_d & z_f & \varphi_f & x_b & y_b & \varphi_{b3} \end{bmatrix} \tag{2}$$

Second Lagrange method is used to derive the equations of motion for tractor/implement system.

$$\frac{\partial}{\partial t}\left(\frac{\partial T}{\partial \dot{\mathbf{q}}_i}\right) - \frac{\partial T}{\partial \mathbf{q}_i} + \frac{\partial U}{\partial \mathbf{q}_i} + \frac{\partial R}{\partial \dot{\mathbf{q}}_i} = \mathbf{Q}_i(t) \tag{3}$$

where T represents the kinetic energy of the tractor/implement system, U is the potential energy, R is the dissipative energy caused by non-potential force, $\mathbf{Q}_i(t)$ is the external generalised force.

The kinetic energy of system can be given by:

$$T = \begin{bmatrix} m_b\left(\dot{z}_b^2 + \dot{x}_b^2 + \dot{y}_b^2\right) + J_{b1}\dot{\varphi}_{b1}^2 + J_{b2}\varphi_{b2}^2 + J_{b3}\varphi_{b3}^2 + m_c\dot{z}_c^2 \\ + J_{c1}\dot{\varphi}_{c1}^2 + J_{c2}\dot{\varphi}_{c2}^2 + m_d\dot{z}_d^2 + m_f\dot{z}_f^2 + J_f\dot{\varphi}_f^2 \end{bmatrix} \Big/ 2 \tag{4}$$

The potential energy of tractor/implement system can be expressed as:

$$\begin{aligned} U = {} & [k_d(z_d - z_c - l_d\varphi_{c1})^2 + k_{cfr}(z_c - l_{cf}\varphi_{c1} - l_{cw}\varphi_{c2} - z_b + l_{bf}\varphi_{b1} + l_{cw}\varphi_{b2})^2 + k_{cfl}(z_c - l_{cf}\varphi_{c1} \\ & + l_{cw}\varphi_{c2} - z_b + l_{bf}\varphi_{b1} - l_{cw}\varphi_{b2})^2 + k_{crr}(z_c + l_{cr}\varphi_{c1} - l_{cw}\varphi_{c2} - z_b - l_{br}\varphi_{b1} + l_{cw}\varphi_{b2})^2 + k_{crl}(z_c + l_{cr}\varphi_{c1} \\ & + l_{cw}\varphi_{c2} - z_b - l_{br}\varphi_{b1} - l_{cw}\varphi_{b2})^2 + k_{sfr}(z_b - l_f\varphi_{b1} - l_{sw}\varphi_{b2} - z_f + l_{sw}\varphi_f)^2 + k_{sfl}(z_b - l_f\varphi_{b1} + l_{sw}\varphi_{b2} \\ & - z_f - l_{sw}\varphi_f)^2 + k_{tz,fr}\left(z_f - l_{bw}\varphi_f - q_{fr}\right)^2 + k_{tz,fl}\left(z_f + l_{bw}\varphi_f - q_{fl}\right)^2 + k_{tz,rr}(z_b + l_r\varphi_{b1} - l_{bw}\varphi_{b2} - q_{rr})^2 \\ & + k_{tz,fl}(z_b + l_r\varphi_{b1} + l_{bw}\varphi_{b2} - q_{rl})^2 + k_{tx,fl}\left(x_b + (r_f - h_b)\varphi_{b1} - l_{bw}\varphi_{b3}\right)^2 + k_{tx,fr}(x_b + (-h_b + r_f)\varphi_{b1} \\ & + l_{bw}\varphi_{b3})^2 + k_{tx,rl}(x_b + (r_r - h_b)\varphi_{b1} - l_{bw}\varphi_{b3}\Big)^2 + k_{tx,rr}(x_b + (r_r - h_b)\varphi_{b1} + l_{bw}\varphi_{b3}\Big)^2 + (k_{ty,fl} + k_{ty,fr}\Big)(y_b \\ & + (h_p - h_a)\varphi_f + (h_b - h_p)\varphi_{b2} + l_{bf}\varphi_{b3})^2 + (k_{ty,rl} + k_{ty,rr})(y_b + (h_b - r_r)\varphi_{b2} - b\varphi_{b3}\Big)^2\Big]/2 \end{aligned} \tag{5}$$



Fig. 3 – Physical wheeled tractor/implement system: (a) three-point hitch, (b) passive rubber suspension of cabin.

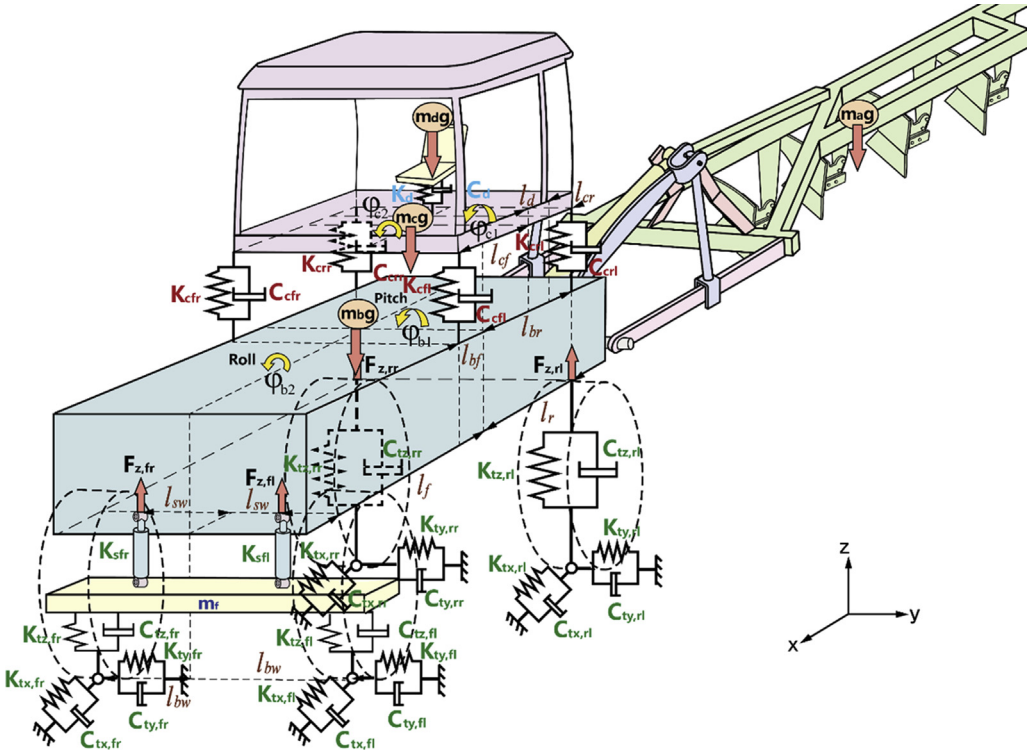


Fig. 4 – Multibody dynamic model of wheeled tractor/implement system with hydro-pneumatic suspension on front axle.

The dissipative energy caused by non-potential force can be calculated as:

When the tractor/implement system travels under transportation condition, the external generalised force is zero.

$$
\begin{aligned}
R = \big[& c_d(\dot{z}_d - \dot{z}_c - l_d\dot{\varphi}_{c1})^2 + c_{cfr}(\dot{z}_c - l_{cf}\dot{\varphi}_{c1} - l_{cw}\dot{\varphi}_{c2} - \dot{z}_b + l_{bf}\dot{\varphi}_{b1} + l_{cw}\dot{\varphi}_{b2})^2 + c_{cfl}(\dot{z}_c - l_{cf}\dot{\varphi}_{c1} \\
& + l_{cw}\dot{\varphi}_{c2} - \dot{z}_b + l_{bf}\dot{\varphi}_{b1} - l_{cw}\dot{\varphi}_{b2})^2 + c_{crr}(\dot{z}_c + l_{cr}\dot{\varphi}_{c1} - l_{cw}\dot{\varphi}_{c2} - \dot{z}_b - l_{br}\dot{\varphi}_{b1} + l_{cw}\dot{\varphi}_{b2})^2 + c_{crl}(\dot{z}_c \\
& + l_{cr}\dot{\varphi}_{c1} + l_{cw}\dot{\varphi}_{c2} - \dot{z}_b - l_{br}\dot{\varphi}_{b1} - l_{cw}\dot{\varphi}_{b2})^2 + c_{sfr}(\dot{z}_b - l_f\dot{\varphi}_{b1} - l_{sw}\dot{\varphi}_{b2} - \dot{z}_f + l_{sw}\dot{\varphi}_f)^2 + c_{sfl}(\dot{z}_b - l_f\dot{\varphi}_{b1} \\
& + l_{sw}\dot{\varphi}_{b2} - \dot{z}_f - l_{sw}\dot{\varphi}_f)^2 + c_{tz,fr}\left(\dot{z}_f - l_{bw}\dot{\varphi}_f - \dot{q}_{fr}\right)^2 + c_{tz,fl}\left(\dot{z}_f + l_{bw}\dot{\varphi}_f - \dot{q}_{fl}\right)^2 + c_{tz,rr}(\dot{z}_b + l_r\dot{\varphi}_{b1} - l_{bw}\dot{\varphi}_{b2} \\
& - \dot{q}_{rr})^2 + c_{tz,fl}(\dot{z}_b + l_r\dot{\varphi}_{b1} + l_{bw}\dot{\varphi}_{b2} - \dot{q}_{rl})^2 + c_{tx,fl}\left(\dot{x}_b + (r_f - h_b)\dot{\varphi}_{b1} - l_{bw}\dot{\varphi}_{b3}\right)^2 + c_{tx,fr}\left(\dot{x}_b + (r_f - h_b)\dot{\varphi}_{b1}\right. \\
& \left. + l_{bw}\dot{\varphi}_{b3}\right)^2 + c_{tx,rl}\left(\dot{x}_b + (r_r - h_b)\dot{\varphi}_{b1} - l_{bw}\dot{\varphi}_{b3}\right)^2 + c_{tx,rr}\left(\dot{x}_b + (r_r - h_b)\dot{\varphi}_{b1} + l_{bw}\dot{\varphi}_{b3}\right)^2 + (c_{ty,fl} + c_{ty,fr})(\dot{y}_b \\
& + (h_p - h_a)\dot{\varphi}_f + (h_b - h_p)\dot{\varphi}_{b2} + l_{bf}\dot{\varphi}_{b3})^2 + (c_{ty,rl} + c_{ty,rr})\left(\dot{y}_b + (h_b - r_r)\dot{\varphi}_{b2} - b\dot{\varphi}_{b3}\right)^2\big]/2
\end{aligned}
\tag{6}
$$

When the second Lagrange method is used, the governing equations of motion for the wheeled tractor/implement system with a hydro-pneumatic suspension on the front axle can be expressed in matrix form:

$$[\mathbf{M}]\ddot{\boldsymbol{q}} + [\mathbf{C}]\dot{\boldsymbol{q}} + [\boldsymbol{K}]\boldsymbol{q} = 0 \tag{7a}$$

where $\mathbf{M}$ represents the mass matrix of the system, $\mathbf{C}$ is the damping matrix of the system, $\boldsymbol{K}$ represents the stiffness matrix. The stiffness and damping matrix coefficients k_{ij}, c_{ij} can be found in Appendix A.

$$\mathbf{M} = \begin{bmatrix}
m_b & 0 & 0 & 0 & 0 & 0 & 0 & 0 & 0 & 0 & 0 & 0 \\
0 & J_{b1} & 0 & 0 & 0 & 0 & 0 & 0 & 0 & 0 & 0 & 0 \\
0 & 0 & J_{b2} & 0 & 0 & 0 & 0 & 0 & 0 & 0 & 0 & 0 \\
0 & 0 & 0 & m_c & 0 & 0 & 0 & 0 & 0 & 0 & 0 & 0 \\
0 & 0 & 0 & 0 & J_{c1} & 0 & 0 & 0 & 0 & 0 & 0 & 0 \\
0 & 0 & 0 & 0 & 0 & J_{c2} & 0 & 0 & 0 & 0 & 0 & 0 \\
0 & 0 & 0 & 0 & 0 & 0 & m_d & 0 & 0 & 0 & 0 & 0 \\
0 & 0 & 0 & 0 & 0 & 0 & 0 & m_f & 0 & 0 & 0 & 0 \\
0 & 0 & 0 & 0 & 0 & 0 & 0 & 0 & J_f & 0 & 0 & 0 \\
0 & 0 & 0 & 0 & 0 & 0 & 0 & 0 & 0 & m_b & 0 & 0 \\
0 & 0 & 0 & 0 & 0 & 0 & 0 & 0 & 0 & 0 & m_b & 0 \\
0 & 0 & 0 & 0 & 0 & 0 & 0 & 0 & 0 & 0 & 0 & J_{c3}
\end{bmatrix},$$

$$\mathbf{K} = \begin{bmatrix}
k_{11} & k_{12} & k_{13} & k_{14} & k_{15} & k_{16} & k_{17} & k_{18} & k_{19} & k_{1,10} & k_{1,11} & k_{1,12} \\
k_{21} & k_{22} & k_{23} & k_{24} & k_{25} & k_{26} & k_{27} & k_{28} & k_{29} & k_{2,10} & k_{2,11} & k_{2,12} \\
k_{31} & k_{32} & k_{33} & k_{34} & k_{35} & k_{36} & k_{37} & k_{38} & k_{39} & k_{3,10} & k_{3,11} & k_{3,12} \\
k_{41} & k_{42} & k_{43} & k_{44} & k_{45} & k_{46} & k_{47} & k_{48} & k_{49} & k_{4,10} & k_{4,11} & k_{4,12} \\
k_{51} & k_{52} & k_{53} & k_{54} & k_{55} & k_{56} & k_{57} & k_{58} & k_{59} & k_{5,10} & k_{5,11} & k_{5,12} \\
k_{61} & k_{62} & k_{63} & k_{64} & k_{65} & k_{66} & k_{67} & k_{68} & k_{69} & k_{6,10} & k_{6,11} & k_{6,12} \\
k_{71} & k_{72} & k_{73} & k_{74} & k_{75} & k_{76} & k_{77} & k_{78} & k_{79} & k_{7,10} & k_{7,11} & k_{7,12} \\
k_{81} & k_{82} & k_{83} & k_{84} & k_{85} & k_{86} & k_{87} & k_{88} & k_{89} & k_{8,10} & k_{8,11} & k_{8,12} \\
k_{91} & k_{92} & k_{93} & k_{94} & k_{95} & k_{96} & k_{97} & k_{98} & k_{99} & k_{9,10} & k_{9,11} & k_{9,12} \\
k_{10,1} & k_{10,2} & k_{10,3} & k_{10,4} & k_{10,5} & k_{10,6} & k_{10,7} & k_{10,8} & k_{10,9} & k_{10,10} & k_{10,11} & k_{10,12} \\
k_{11,1} & k_{11,2} & k_{11,3} & k_{11,4} & k_{11,5} & k_{11,6} & k_{11,7} & k_{11,8} & k_{11,9} & k_{11,10} & k_{11,11} & k_{11,12} \\
k_{12,1} & k_{12,2} & k_{12,3} & k_{12,4} & k_{12,5} & k_{12,6} & k_{12,7} & k_{12,8} & k_{12,9} & k_{12,10} & k_{12,11} & k_{12,12}
\end{bmatrix}$$

$$\mathbf{C} = \begin{bmatrix}
c_{11} & c_{12} & c_{13} & c_{14} & c_{15} & c_{16} & c_{17} & c_{18} & c_{19} & c_{1,10} & c_{1,11} & c_{1,12} \\
c_{21} & c_{22} & c_{23} & c_{24} & c_{25} & c_{26} & c_{27} & c_{28} & c_{29} & c_{2,10} & c_{2,11} & c_{2,12} \\
c_{31} & c_{32} & c_{33} & c_{34} & c_{35} & c_{36} & c_{37} & c_{38} & c_{39} & c_{3,10} & c_{3,11} & c_{3,12} \\
c_{41} & c_{42} & c_{43} & c_{44} & c_{45} & c_{46} & c_{47} & c_{48} & c_{49} & c_{4,10} & c_{4,11} & c_{4,12} \\
c_{51} & c_{52} & c_{53} & c_{54} & c_{55} & c_{56} & c_{57} & c_{58} & c_{59} & c_{5,10} & c_{5,11} & c_{5,12} \\
c_{61} & c_{62} & c_{63} & c_{64} & c_{65} & c_{66} & c_{67} & c_{68} & c_{69} & c_{6,10} & c_{6,11} & c_{6,12} \\
c_{71} & c_{72} & c_{73} & c_{74} & c_{75} & c_{76} & c_{77} & c_{78} & c_{79} & c_{7,10} & c_{7,11} & c_{7,12} \\
c_{81} & c_{82} & c_{83} & c_{84} & c_{85} & c_{86} & c_{87} & c_{88} & c_{89} & c_{8,10} & c_{8,11} & c_{8,12} \\
c_{91} & c_{92} & c_{93} & c_{94} & c_{95} & c_{96} & c_{97} & c_{98} & c_{99} & c_{9,10} & c_{9,11} & c_{9,12} \\
c_{10,1} & c_{10,2} & c_{10,3} & c_{10,4} & c_{10,5} & c_{10,6} & c_{10,7} & c_{10,8} & c_{10,9} & c_{10,10} & c_{10,11} & c_{10,12} \\
c_{11,1} & c_{11,2} & c_{11,3} & c_{11,4} & c_{11,5} & c_{11,6} & c_{11,7} & c_{11,8} & c_{11,9} & c_{11,10} & c_{11,11} & c_{11,12} \\
c_{12,1} & c_{12,2} & c_{12,3} & c_{12,4} & c_{12,5} & c_{12,6} & c_{12,7} & c_{12,8} & c_{12,9} & c_{12,10} & c_{12,11} & c_{12,12}
\end{bmatrix}, \tag{7b}$$

$$\mathbf{Q} = \begin{bmatrix} Q_1 \\ Q_2 \\ Q_3 \\ Q_4 \\ Q_5 \\ Q_6 \\ Q_7 \\ Q_8 \\ Q_9 \\ Q_{10} \\ Q_{11} \\ Q_{12} \end{bmatrix} = \begin{bmatrix} k_{tz,rr}q_{rr} + k_{tz,rl}q_{rl} + c_{tz,rr}\dot{q}_{rr} + c_{tz,rl}\dot{q}_{rl} \\ k_{tz,rr}l_r q_{rr} + k_{tz,rl}l_r q_{rl} + c_{tz,rr}l_r\dot{q}_{rr} + c_{tz,rl}l_r\dot{q}_{rl} \\ -k_{tz,rr}l_{bw}q_{rr} + k_{tz,rl}l_{bw}q_{rl} - c_{tz,rr}l_{bw}\dot{q}_{rr} + c_{tz,rl}l_{bw}\dot{q}_{rl} \\ 0 \\ 0 \\ 0 \\ 0 \\ k_{tz,fr}q_{fr} + k_{tz,fl}q_{fl} + c_{tz,fr}\dot{q}_{fr} + c_{tz,fl}\dot{q}_{fl} \\ -k_{tz,fr}l_{bw}q_{fr} + k_{tz,fl}l_{bw}q_{fl} - c_{tz,fr}l_{bw}\dot{q}_{fr} + c_{tz,fl}l_{bw}\dot{q}_{fl} \\ 0 \\ 0 \\ 0 \end{bmatrix}$$

3.1. Model of front axle hydro-pneumatic suspension

The function of the large throttle valve 10 is to increase the volume of accumulator A. In practice, the large throttle valve 10 is often closed and the effect of accumulator C can be neglected. Then, the model of the front axle hydro-pneumatic suspension is developed shown in Fig. 2. It is assumed that the compressibility of oil can be neglected compared with that of the nitrogen in accumulator. The force caused by the piston rod can be expressed as:

$$F_h = P_1A_1 - P_2A_2 \tag{8}$$

where P_1 and P_2 represent the transient pressure in the rod and rodless cavity, respectively, $A_1$is the area of piston, $A_1 = \frac{\pi D^2}{4}$, D represents the diameter of the piston, A_2 is the effective area of the rod cavity, $A_2 = \frac{\pi(D^2-d^2)}{4}$, d is the diameter of the piston rod.

The length of orifice in the throttle and proportional valves of the hydro-pneumatic suspension is very short and its oil flow can be calculated as:

$$q = C_dA\sqrt{\frac{2\Delta P}{\rho}} \tag{9}$$

where ρ represents the density of oil, A is the flow area of hole for the throttle and proportional valves, C_d is the flow coefficient of hole, ΔP represents the pressure difference between oil cavity and the accumulator.

When the hydro-pneumatic suspension is compressed, the oil in the rodless cavity 1 flows to the accumulator A through the throttle valve 6 and the proportional valve 5, the oil in the accumulator B flows to the rod cavity 2 through the throttle valve 8 and the proportional valve 7. Similarly, when the hydro-pneumatic suspension is rebounded, the oil flow direction is opposite. The relationship between the flow and the velocity of piston rod can be given by:

$$\begin{cases} A_1\dot{x} = \mathrm{sgn}(\dot{x})C_dA_9\sqrt{\frac{2\Delta P_{21}}{\rho}} + \mathrm{sgn}(\dot{x})C_d(A_5+A_6)\sqrt{\frac{2\Delta P_{A1}}{\rho}} \\ A_2\dot{x} = \mathrm{sgn}(\dot{x})C_dA_9\sqrt{\frac{2\Delta P_{21}}{\rho}} + \mathrm{sgn}(\dot{x})C_d(A_7+A_8)\sqrt{\frac{2\Delta P_{2B}}{\rho}} \end{cases} \tag{10}$$

where A_6 and A_8 represent the flow area of the throttle valves 6 and 8, respectively, A_5 and A_7 are the flow area of the proportional valves 5 and 7, A_9 is the flow area of the throttle valve 9, ΔP_{1A} is the absolute oil pressure difference between the rodless cavity 1 and the accumulator A, ΔP_{2B} is the absolute oil pressure difference between the rod cavity 2 and accumulator B, $\mathrm{sgn}(\dot{x})$ represents the symbolic function, $\dot{x}$represents the relative velocity between the chassis and the front axle, $\dot{x} = \dot{z}_b - l_f\dot{\varphi}_b - \dot{z}_e$.

The symbolic function can be described as:

$$\mathrm{sgn}(\dot{x}) = \begin{cases} 1 & \dot{x} > 0 \\ 0 & \dot{x} = 0 \\ -1 & \dot{x} < 0 \end{cases} \tag{11}$$

The relationship between the volume change of accumulators A and B with respect to time and the oil flow of throttle and proportional valves can be given by:

$$\begin{cases} \mathrm{sgn}(\dot{x})C_d(A_5+A_6)\sqrt{\frac{2\Delta P_{A1}}{\rho}}dt = \dot{V}_A \\ \mathrm{sgn}(\dot{x})C_d(A_7+A_8)\sqrt{\frac{2\Delta P_{2B}}{\rho}}dt = -\dot{V}_B \end{cases} \tag{12}$$

The gas in the accumulator is considered to be ideal and the temperature of gas keeps constant. The state equations of ideal gas can be described as:

$$P_AV_A = P_{A0}V_{A0},\ P_BV_B = P_{B0}V_{B0} \tag{13}$$

where P_A and V_A are the transient pressure and the volume of accumulator A, respectively, P_B and V_B are the transient pressure and the volume of accumulator B, P_{A0} and V_{A0} are the initial pressure and the initial volume of accumulator A, P_{B0} and V_{B0} are the initial pressure and the initial volume of accumulator B.

Based on the state equations of the ideal gas, the oil pressure of the accumulators A and B can be calculated by:

$$P_A = \frac{P_{A0}V_{A0}}{(V_{A0}-A_1x)},\ P_B = \frac{P_{B0}V_{B0}}{(V_{B0}+A_2x)} \tag{14}$$

where x represents the relative displacement between chassis and front axle, $x = z_b - l_f\varphi_b - z_e$.

By differentiating Eq. (13) with respect to time, the volume change of accumulators A and B with respect to time can be obtained.

$$\begin{cases} \dot{V}_A = \frac{(-P_{A0}V_{A0}\dot{P}_A)}{P_A^2} \\ \dot{V}_B = \frac{(-P_{B0}V_{B0}\dot{P}_B)}{P_B^2} \end{cases} \tag{15}$$

By solving the Eq. (10), the oil pressure can be obtained as:

$$\begin{cases} P_1 = P_A - \frac{\left[\rho P_{A0}^2V_{A0}^2(\dot{P}_A/P_A)^2\mathrm{sgn}(\dot{x})\right]}{\left[2C_d^2(A_5+A_6)^2\right]} \\ P_2 = P_B + \frac{\left[\rho P_{B0}^2V_{B0}^2(\dot{P}_B/P_B)^2\mathrm{sgn}(\dot{x})\right]}{\left[2C_d^2(A_7+A_8)^2\right]} \end{cases} \tag{16}$$

Friction force between the cylinder and the piston can be expressed as:

$$F_f(\dot{x}) = \mathrm{sgn}(\dot{x})\left[F_c + (F_s - F_c)e^{-\left(\frac{\dot{x}}{\dot{x}_S}\right)^2} + f_v\dot{x}\right] \tag{17}$$

where F_c represents the Coulomb friction force, F_s is the static friction force, f_v is the coefficient of viscous friction force, $\dot{x}_s$ is the Stribeck velocity that is an empirical parameter.

Therefore, the total force on the piston rod considering the effect of damping force of orifice and friction between the cylinder and piston can be given by:

$$F_p = F_h - F_f \tag{18}$$

Actually, the state of the throttle valve 9 is either closed or fully opened when the hydro-pneumatic suspension is

applied to the front axle of tractor system. When the throttle valve 9 is closed, the force of the hydro-pneumatic suspension can be calculated as:

$$F_p = \frac{\rho A_1{}^3 \dot{x}^2 \mathrm{sign}(\dot{x})}{2C_d^2(A_j + A_c)^2} + \frac{P_{A0}V_{A0}^r A_1}{(V_{A0} - A_1 x)^r} - \mathrm{sign}(\dot{x})\left[F_c + (F_s - F_c)e^{-\left(\frac{\dot{x}}{\dot{x}_s}\right)^2} + F_v\dot{x}\right] - \frac{P_{B0}V_{B0}^r A_2}{(V_{B0} + A_2 x)^r} + \frac{\rho A_2^3 \dot{x}^2 \mathrm{sign}(\dot{x})}{2C_d^2(A_z + A_d)^2} \quad (19)$$

When the throttle valve 9 is fully opened, the force of the hydro-pneumatic suspension can be calculated as:

$$F_p = \frac{P_{A0}(V_{A0} + V_{B0})(A_1 - A_2)}{[P_{A0}(V_{A0} + V_{B0})(A_1 - A_2)/(Mg) - (A_1 - A_2)x]} + [\frac{\rho(A_1 - A_2)^3\dot{x}^2}{4C_d^2(A_5 + A_6)^2} + \frac{\rho(A_1 - A_2)^3\dot{x}^2}{4C_d^2(A_7 + A_8)^2}]\mathrm{sign}(\dot{x}) - \mathrm{sign}(\dot{x})\left[F_c + (F_s - F_c)e^{-\left(\frac{\dot{x}}{\dot{x}_s}\right)^2} + F_v\dot{x}\right] \quad (20)$$

3.2. *Determination of parameters for tractor system*

(1) Pitch, roll and yaw moment of inertia for chassis and cabin

The pitch and roll moment of inertia around the mass centre are important parameters of the tractor, which have a significant influence on the operation stability and the ride comfort of the tractor. Based on the measurement principle of the free attenuation method for single pendulum with blade and spring, the system for measuring the rotary inertia of tractor is constructed, as shown in Fig. 5. A detachable semi-frame is designed on both left and right sides of the tractor. The longitudinal, lateral and vertical length of the frame can be changed by adjusting device. A flange plate is fixed at both ends of the frame, which is rigidly connected with the hub of the front and rear wheels, respectively. The measured body that includes the tractor and two half frames is supported on a rectangular bracket with two blade springs.

When measuring the pitching moment of inertia, the front beam of the two semi-frame is placed on the spring and the back beam is supported by the blade of the semi-frame, as shown in Fig. 5(a). Similarly, when measuring the roll inertia, the left half frame is supported on the spring and the right half frame is supported by the blade, as shown in Fig. 5(b).

The tractor is in a horizontal state supported by a blade and a spring. The spring used in this test is a steel spiral spring, and the stiffness of the semi-frame is large enough so that the effect of the damping of the spring and the deformation of the semi-frame can be neglected. The differential equation of the measurement system under free vibration can be given by:

$$J_{FO}\ddot{\beta} + KL^2\beta = 0 \quad (21)$$

where β represents the swing angle of the measured body (tractor + semi-frame) around the blade, J_{FO} is the inertia moment of the measured body, K is the stiffness of spring, L is the distance between the spring fulcrum and the blade.

The period of the test system can be given by:

$$T = 2\pi\sqrt{\frac{J_{FO}}{(L^2K)}} \quad (22)$$

Based on the vibration period of the test system, the inertia moment of the measured body can be obtained by

$$J_{FO} = \frac{T^2KL^2}{(4\pi^2)} \quad (23)$$

The inertia moment J_{TO} of the tractor around the blade can be expressed as:

$$J_{TO} = J_{FO} - J_{JO} \quad (24)$$

where J_{JO} represents the inertia moment of the semi-frame around the blade.

Based on the parallel axis theorem, the moment of inertia J_C of the tractor system around mass centre can be calculated as:

$$J_C = J_{TO} - M\rho^2 \quad (25)$$

where ρ represents the distance between mass centre of tractor and blade, M is the mass of tractor.

The aforementioned measurement system was assembled at Jiangsu Agricultural Machinery Appraisal Station, as shown in Fig. 6. During the measurement, an external force is applied to compress the support spring of the test frame. Once the force is withdrawn, the tractor oscillates around the blade under the action of the spring force, then the pitch and roll vibrations are measured by the acceleration sensors, respectively.

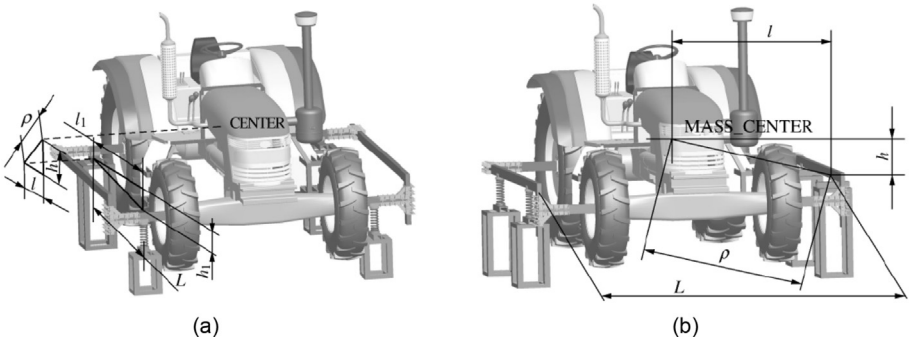


Fig. 5 – The measurement system of the inertia moment of tractors: (a) pitch, (b) roll.



(a) (b)

Fig. 6 – Experimental rig for measuring the inertia moment of tractors: (a) pitch, (b) roll.

The period of the pitch and roll vibration can be obtained from its corresponding acceleration response curves, respectively. To improve the measurement accuracy, the test is repeated three times and the average value is taken. Then, the moment of inertia for tractor around the mass centre can be obtained from Eq. (25).

To obtain the pitch and roll moment of inertia for cabin, the three dimensional solid model of tractor cabin is established in the Pro/E software, as shown in Fig. 7. When the density of steel and glass was applied to the solid model, the pitch and roll moment of inertia for cabin can be determined. Similarly, the yaw moment of inertia for the chassis can be determined by the same method in this work.

(2) Stiffness and damping of tyre, driver seat and rubber suspension of cabin

To derive the vertical stiffness and damping, the tyre is regarded as a single degree of freedom system. Based on the logarithmic decrement method of free vibration, the vertical stiffness and the damping of the front and rear tyres can be achieved. As shown in Fig. 8, the structure of the test rig consists of support frame (1), rope (6), linear bearing (16), beam (7), weight plate (3), ground (14), guide rods (17), acceleration sensor (2), tyre connection plate (15), rings (4), linear bearing beam (8), tyre (5), suction plate (11), holder of displacement sensor (10), displacement sensor (9), magnetic lifter (13), suspension bracket of magnetic lifter (12).

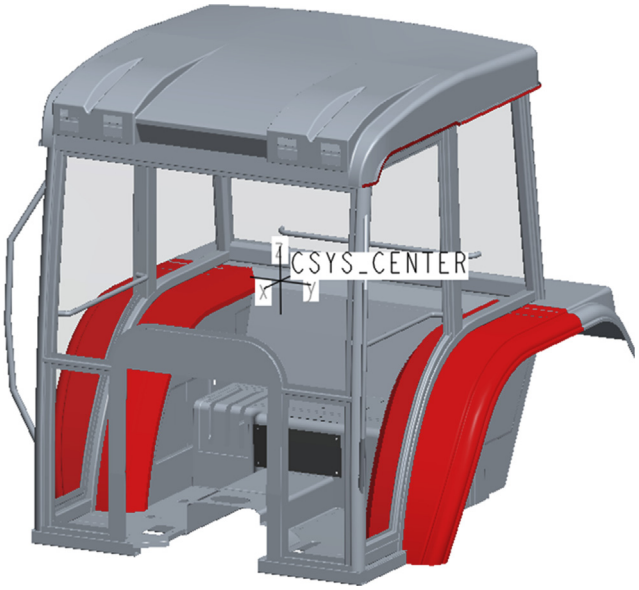


Fig. 7 – Three dimensional solid model of cabin.

The support frame includes column, upper and lower rectangular frames, the linear bearing beam is fixed on the column. Linear bearing is mounted on the beam of guide sleeve bearing, and the measured tyre is installed on the beam through tyre connection plate. The load on the tyre is executed by adding the corresponding weight plates, and the guide rods are connected with the beam through the linear bearing. The one end of the rope through the rings, fixing on the upper and lower frame, is used to lift the measured tyre, and the other end of the rope is connected with the suction plate. The suction plate is adsorbed on the lower surface of the magnetic lifter which is fixed on the suspension bracket. To carry out the experiment of free attenuation on the measured tyre under gravity, the switch of magnetic lifter is controlled by the operator. By changing the height of linear bearing beam on column, the test rig can be used to measure tyres with different diameters. Based on the virtual instrument of vibration testing system, the vibration acceleration signal of tyre is collected using data acquisition card. The software of the test system was written using LabVIEW (National Instruments, Austin, TX, USA), and data acquisition, display and storage was controlled using a virtual instrument panel.

When the tyre is lifted from ground with height h and the magnetic switch is off, the lower beam with guide rods falls freely along the guide sleeve under gravity. After the tyre knocks the ground, the free attenuation vibration starts and its vibrational time history is obtained by the acceleration sensor attached on the beam. The logarithmic decrement can be calculated as:

$$\delta = \frac{1}{j-i}\ln\frac{A_i}{A_j} = \frac{1}{j-i}\ln\frac{\ddot{z}_i}{\ddot{z}_j} \tag{26}$$

The damping ratio can be obtained based on the logarithmic decrement and is given by:

$$\xi = \frac{\delta}{\sqrt{\delta^2 + (2\pi)^2}} \tag{27}$$

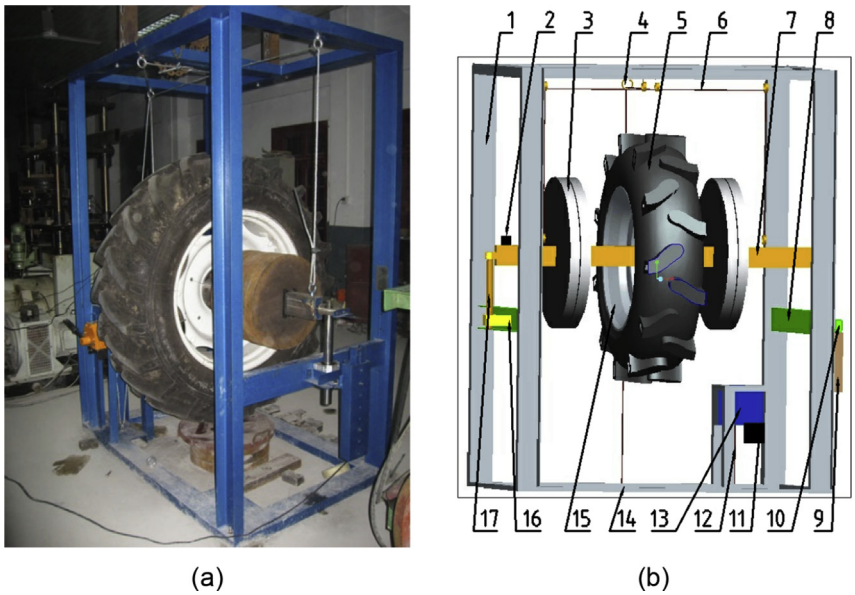


Fig. 8 – Test system of vertical stiffness and damping for tyres: (a) site map, (b) structure.

Then, the vertical stiffness and damping of tyre can be given by:

$$k = \left(\frac{2\pi}{T}\right)^2 \frac{m}{1-\xi^2},\ c = 2\xi\sqrt{km} \tag{28}$$

As the velocity of tractor is very low, the influence of the velocity on the longitudinal and lateral damping of agricultural tractor tyres has to be considered (Lines and Murphy, 1991a, b). The measured vertical stiffness and damping of the front and rear tyres with respect to speed is shown in Fig. 9.

The generation of the longitudinal tyre force requires a slip in X direction,γ, defined as (Crolla, Horton, & Stayner, 1990):

$$\gamma = \frac{r\dot{\theta} - \dot{x}}{v} \tag{29}$$

where r represents the radius of tyre, $\dot{x}$ is the longitudinal tyre speed, $\dot{\theta}$ is the roll speed of tyre, v is the forward speed.

A first order lag is introduced to describe the tyre's dynamic response.

$$\frac{\sigma_\gamma}{v}\dot{F}_x + F_x = C_\gamma \gamma \tag{30}$$

Thus, the longitudinal tyre force model can be considered as a spring and a damper connected in series.

$$k_x = \frac{C_\gamma}{\sigma_\gamma},\ c_x = \frac{C_\gamma}{v} \tag{31}$$

Similarly, the lateral tyre force generation also needs a slip angle, which can be given by:

$$\alpha = \frac{-\dot{y}}{v} \tag{32}$$

where $\dot{y}$ represents the lateral tyre speed.

The first order lag is also introduced to describe the tyre's dynamic response.

$$\frac{\sigma_\alpha}{v}\dot{F}_y + F_y = C_\alpha \beta \tag{33}$$

The lateral tyre force model can be considered as a spring and a damper connected in series.

$$k_y = \frac{C_\alpha}{\sigma_\alpha},\ c_y = \frac{C_\alpha}{v} \tag{34}$$

The measured longitudinal and lateral stiffness, damping of the front and rear tyres are supplied by the tractor manufacturer, as listed in Table 1.

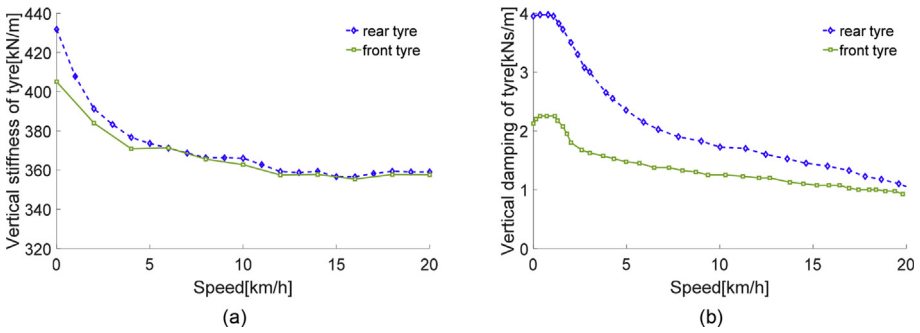


Fig. 9 – Measured vertical stiffness and damping of front and rear tyres with respect to speed: (a) stiffness, (b) damping.

Table 1 – Parameters of wheeled tractor/implement with front axle hydro-pneumatic suspension.

l_f	1348 mm	l_{cf}	600 mm	m_c	375 kg
	840 mm	l_{cr}	290 mm	m_d	75 kg
	360 mm	l_d	290 mm	J_{b1}	3249 kg m^2
	840 mm	m_b	2694 kg	J_{c1}	219 kg m^2
$k_{tz,fl}$,$k_{tz,fr}$	357,177 N/m	$c_{tz,fl}$,$c_{tz,fr}$	1789 N s/m	$k_{tz,rl}$,$k_{tz,rr}$	359,304 N m^{-1}
$c_{tz,rl}$,$c_{tz,rr}$	2517 N s/m	k_{cfl},k_{crr}	1,012,383 N/m	c_{cfl},c_{crr}	5093 N s m^{-1}
k_{crl},k_{crr}	1,012,383 N/m	c_{crl},c_{crr}	5093 N s/m	A_7+A_8	4.52 × 10^{-6} m^2
	1473 N s/m	m_a	300 kg	m_f	240 kg
	19,800 N/m	J_{b2}	2085 kg m^2	J_{b3}	4334 kg m^2
	254 kg m^2	J_{c2}	200 kg m^2	l_{sw}	500 mm
	300 mm	l_{bw}	866 mm	h_b	955 mm
	580 mm	h_p	680 mm	r_f	580 mm
	700 mm	$c_{ty,fl}$,$c_{ty,fr}$	1789 N s/m	$c_{ty,rl}$,$c_{ty,rr}$	1159 N s m^{-1}
$k_{tx,fl}$,$k_{tx,fr}$	757,000 N/m	$k_{tx,rl}$,$k_{tx,rr}$	823,000 N/m	$k_{ty,fl}$,$k_{ty,fr}$	208,000 N m^{-1}
$k_{ty,rl}$,$k_{ty,rr}$	218,000 N/m	$c_{tx,fl}$,$c_{tx,fr}$	3013 N s/m	$c_{tx,rl}$,$c_{tx,rr}$	2418 N s m^{-1}
	2994 kg	D	0.05 m	d	0.032 m
	0.7	ρ	900 kg/m^3	A_5+A_6	4.52 × 10^{-6} m^2
	0 m^2	P_{A0}	6 MPa	V_{A0}	0.5 l
	6 MPa	V_{B0}	0.5 L	F_c	100 N
	220 N	f_v	2	$\dot{x}_s$	0.003 m s^{-1}

The nonlinear vertical stiffness and damping of the rubber suspension for cabin change with the excitation amplitude and frequency, which can be expressed as:

$$k_c = \frac{m\omega^2(\alpha^2 - \alpha\cos\varphi)}{\alpha^2 - 2\alpha\cos\varphi + 1} \tag{35a}$$

$$c_c = \frac{m\omega\alpha\sin\varphi}{\alpha^2 - 2\alpha\cos\varphi + 1} \tag{35b}$$

where α represents the ratio of the output acceleration amplitude with respect to the input acceleration amplitude, ω is the frequency of excitation, m is the mass of vibration object, φ is the phase difference between output and input acceleration.

The test site maps of vertical stiffness and damping for the rubber suspension of cabin and driver seat are shown in Figs. 10 and 11, respectively, the measured vertical stiffness and damping of rubber suspension for cabin and driver seat are shown in Figs. 12 and 13. The stiffness and damping of the rubber suspension and driver seat decrease with the increase of the excitation frequency. The mean value of the measured modal stiffness and damping in the frequency range from 4 to 8 Hz, which is the frequency band that the bodies of drivers are sensitive to, can be used in the following simulation.

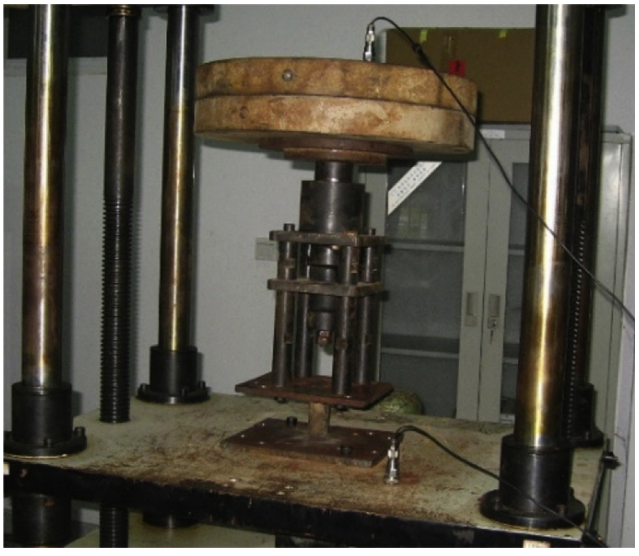


Fig. 10 – Measurement of vertical stiffness and damping for the rubber suspension of cabin.

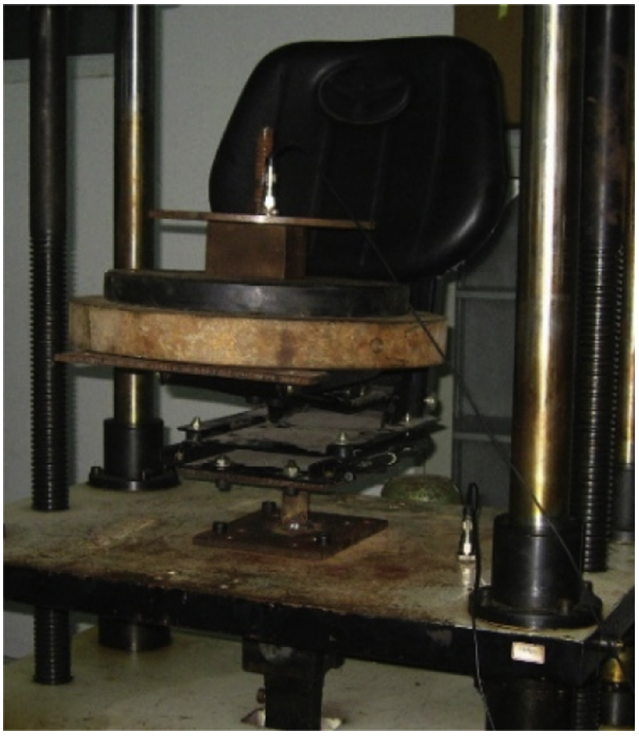


Fig. 11 – Measurement of vertical stiffness and damping for the driver seat.

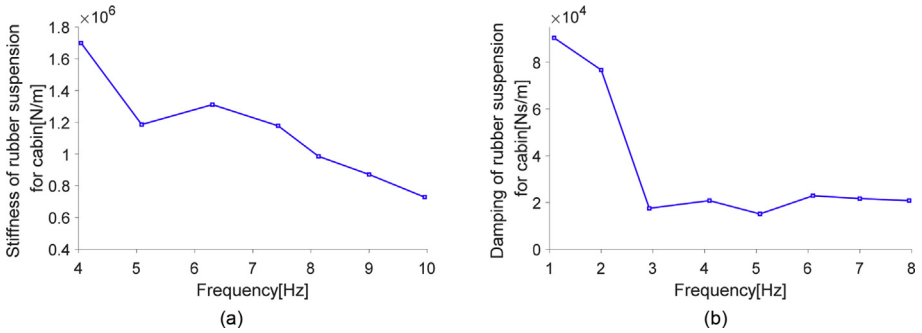


Fig. 12 – Measured stiffness and damping of rubber suspension for cabin: (a) stiffness, (b) damping.

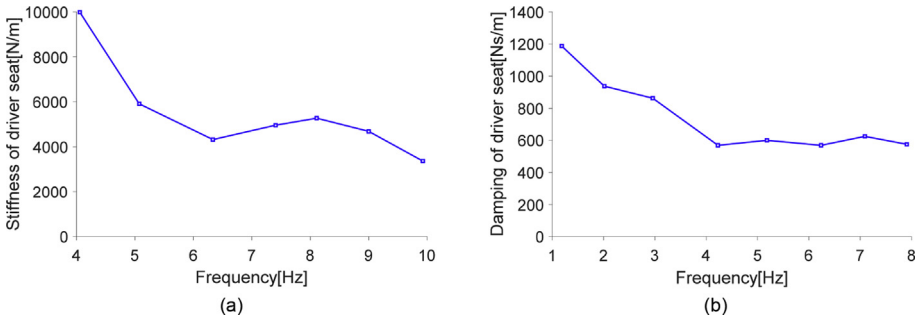


Fig. 13 – Measured stiffness and damping of driver seat: (a) stiffness, (b) damping.

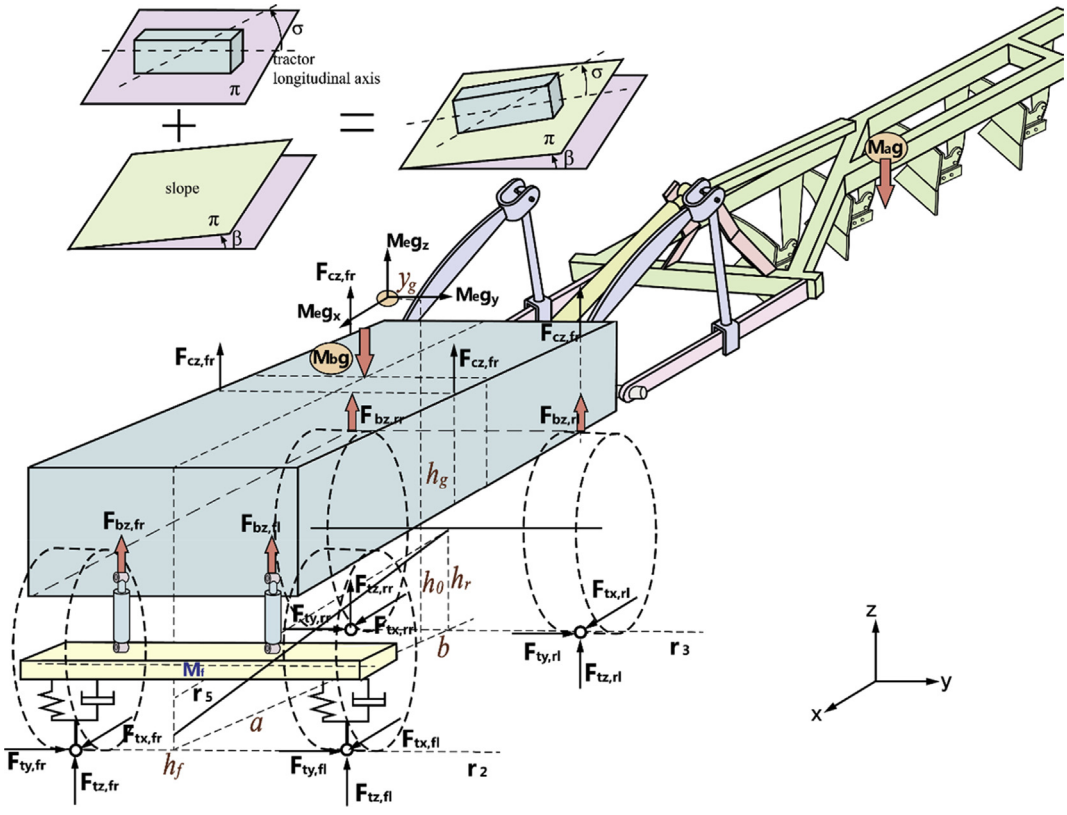


Fig. 14 – Rollover model of wheeled tractor/implement system with suspended front axle.

3.3. Rollover model of tractor with suspended front axle and deformable tyres

To evaluate the handling performances of the wheeled tractor with the influence of the front axle hydro-pneumatic suspension, we assume that the farm tractor rests on a sloped plane. The angle for the situation that one wheel of the farm tractor is lifted is computed in this work. The altitude of the farm tractor with respect to the slope is defined as the angle σ and the inclination of the slope is defined as the angle β (Previati, Gobbi, & Mastinu, 2014). The rollover model of the wheeled tractor/implement system with a suspended front axle on the slope is developed, as shown in Fig. 14. It is also assumed that the chassis is rigidly connected with the implement in the rollover model.

The moment equilibrium relationship with respect to the axle r_2 can be given by:

$$F_{tz,rl}p + F_{tz,rr}p + m_e g_x h + m_e g_z l_{bf} + (F_{cz,fl} + F_{cz,fr})(l_f - l_{bf}) + (F_{cz,rl} + F_{cz,rr})(l_f + l_{br}) = 0 \quad (36)$$

where $h = (h_g - h_0)\cos\rho_r + h_0 + y_g \sin\rho_r$.

The moment equilibrium relationship of the tractor body and the rear axle with respect to the axle r_5 can be described as:

$$F_{tz,rl}\left(t_{rl} + \tan\beta \sin\sigma(h_f - h_r + h_{rl}) \times\right) + F_{tz,fr}\left(-t_{fr} + \tan\beta \sin\sigma(h_f - h_r + h_{rr}) \times\right) - m_e g_y h + m_e g_z y + M_a + (F_{cz,fl} + F_{cz,rl})l_{cw} - (F_{cz,fr} + F_{cz,rr})l_{cw} = 0 \quad (37)$$

where $y = -(h_g - h_0)\sin\rho_r + y_g \cos\rho_r, h_{rl} = h_r \cos\rho_r + t_{rl} \sin\rho_r, h_{rr} = h_r \cos\rho_r - t_{rr} \sin\rho_r$.

The relationship between the roll angle and the forces on the two rear tyres in the vertical direction can be expressed as:

$$F_{tz,rl} - F_{tz,rr} - k_r(h_{rl} - h_{rr}) = 0 \quad (38)$$

The moment equilibrium relationship with respect to the axle r_3 can be given by:

$$F_{tz,fl}p + F_{tz,fr}p - m_e g_x h + M_e g_z l_{br} + (F_{cz,fl} + F_{cz,fr})(l_r + l_{bf}) + (F_{cz,rl} + F_{cz,rr})(l_r - l_{br}) = 0 \quad (39)$$

The moment equilibrium of the front axle with respect to the axle r_5 can be described as:

$$F_{ty,fl}t_{fl} + F_{ty,fl}h_{fl} - F_{tz,fr}t_{fr} + F_{ty,fr}h_{fr} + (F_{cz,fl} + F_{cz,rl})l_{cw} - (F_{cz,fr} + F_{cz,rr})l_{cw} = 0 \quad (40)$$

where $h_{fl} = h_f \cos\rho_f + t_f \sin\rho_f, h_{fr} = h_f \cos\rho_f - t_f \sin\rho_f$.

The relationship between the roll angle and the forces on the two front tyres in the vertical direction can be expressed as:

$$F_{tz,fl} - F_{tz,fr} - k_f(h_{fl} - h_{fr}) = 0 \quad (41)$$

A set of state variables selected for this analysis are listed below:

$$u_1 = z_b,\ u_2 = \varphi_{b1},\ u_3 = \varphi_{b2},\ u_4 = z_c,\ u_5 = \varphi_{c1},\ u_6 = \varphi_{c2},\ u_7 = z_d,\ u_8 = z_f,\ u_9 = \varphi_f,\ u_{10} = x_b,\ u_{11} = y_b,\ u_{12} = \varphi_{b3} \quad (42a)$$

$$u_{13} = z_b,\ u_{14} = \varphi_{b1},\ u_{15} = \varphi_{b2},\ u_{16} = z_c,\ u_{17} = \varphi_{c1},\ u_{18} = \varphi_{c2},\ u_{19} = z_d,\ u_{20} = z_f,\ u_{21} = \varphi_f,\ u_{22} = x_b,\ u_{23} = y_b,\ u_{24} = \varphi_{b3} \quad (42b)$$

By substituting Eqs. (42a) and (42b) into Eqs. (7a) and (7b), the second-order differential equations can be reduced to the first-order differential equations, which allows easy mathematical handling. Numerical solutions with higher precision can be achieved using the fourth-order Runge-Kutta method.

4. Results and discussion

The CF700 wheeled tractor system with an implement and front axle hydro-pneumatic suspension as well as a passive rubber cabin suspension is taken as an example, its structural parameters are shown in Table 1. The standard artificial test track with the length of 100 m is used to simulate the real road, as shown in Fig. 15.

When the forward speed of the tractor is 2 m/s, the nitrogen pressure and the volume of the accumulators A and B are 6 MPa and 0.5 L, the measured and the predicted acceleration of driver seat, cabin, chassis and implement with the orifice diameter 2.4 mm of throttle valves 6 and 8, and 0 mm of throttle valve 9 (closed) of front axle hydro-pneumatic suspension are shown in Fig. 16. Their corresponding PSD are shown in Fig. 17.

It can be seen in Figs. 16 and 17 that there are slight differences between the time series gathered from simulation and the measured values generally. The vibration responses generated by the proposed model agree with experimental results, as a result, the validity of the presented model in this work is verified. To prove the proposed model in this work further, the experimental and the predicted RMS of the acceleration results of the tractor under different forward speed and field road conditions are compared and listed in Tables 2 and 3, respectively.

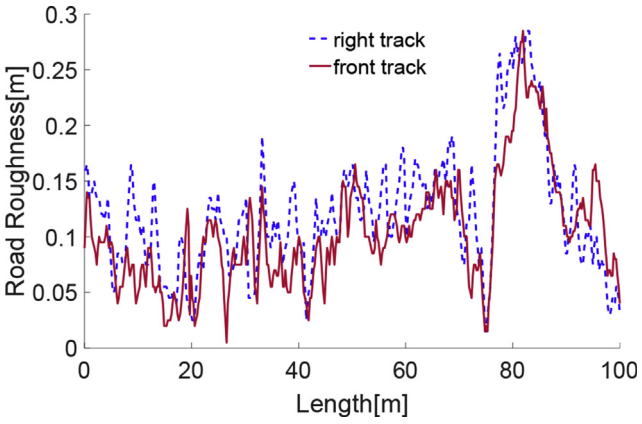


Fig. 15 – Standard road excitation.

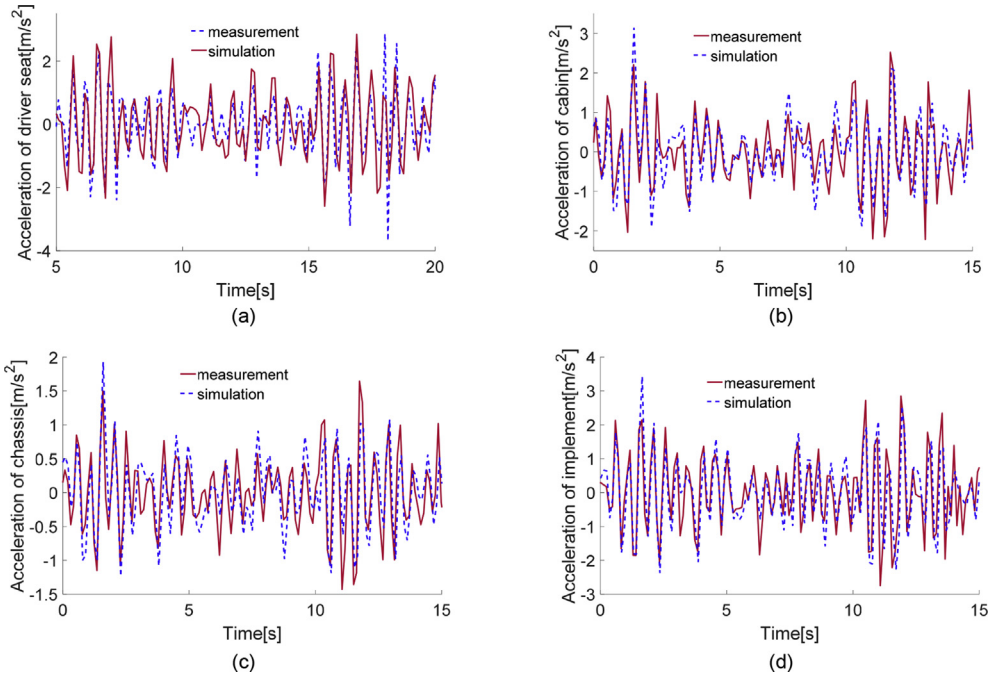


Fig. 16 – Measured and predicted acceleration of tractor system: (a) driver seat, (b) cabin, (c) chassis, (d) implement.

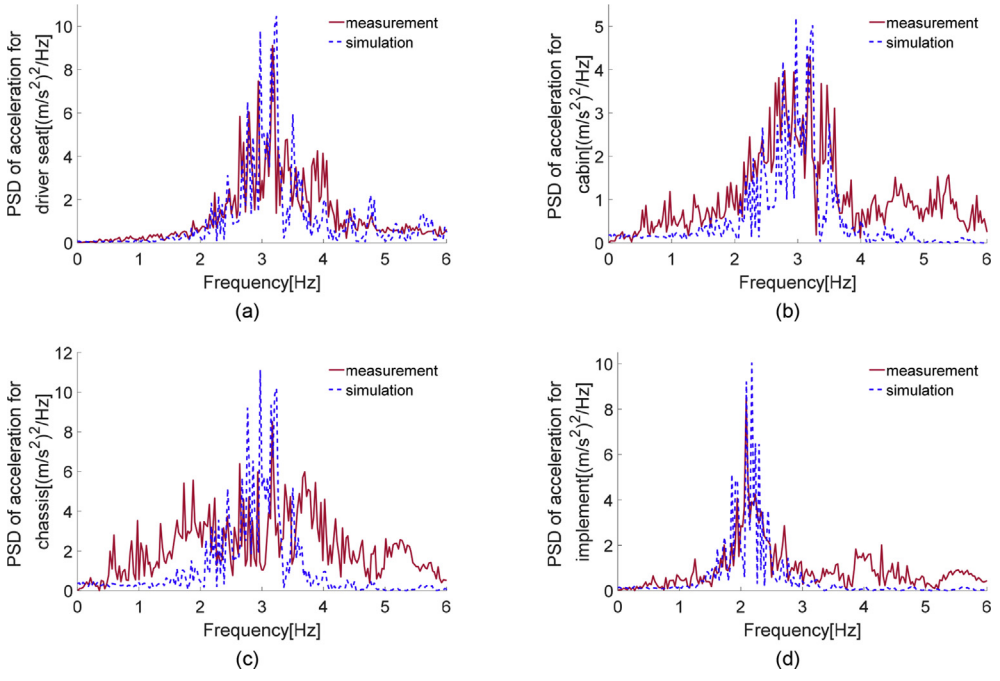


Fig. 17 – Measured and predicted PSD of acceleration: (a) driver seat, (b) cabin, (c) chassis, (d) implement.

It is shown in Tables 2 and 3 that the presented model is also effective in predicting the vibration characteristics of the tractor system. With the increase of the forward speed of the tractor, the RMS of the acceleration responses of driver seat, cabin, chassis and implement increase dramatically. Due to the passive rubber suspension between cabin and chassis, the RMS of the acceleration of cabin is less than that of driver seat, chassis and implement. The RMS of the acceleration responses of driver seat, cabin, chassis and implement under rough standard road are larger than those under rice straw and paddy fields, which indicates that rice straw and paddy soil can act as a vibration suspension for a tractor implement system.

The effect of passive cabin suspension, implement and front axle hydro-pneumatic suspension on the vibration characteristics of tractor system, dynamic models of tractor system under four cases are compared. The four cases are:

Table 2 – Experimental and predicted RMS acceleration of tractor under different forward speed.

Forward speed	driver seat (m s^{-2})			cabin (m s^{-2})		
	Measured	Simulated	%Error	Measured	Simulated	%Error
1.21 m s^{-1}	1.528	1.556	1.83	1.371	1.432	4.45
1.69 m s^{-1}	2.161	2.117	2.04	1.569	1.758	12.05
2.05 m s^{-1}	2.474	2.596	4.93	1.995	2.231	11.83
3.10 m s^{-1}	3.237	3.551	9.70	2.573	2.961	15.08
Forward speed	chassis (m s^{-2})			implement (m s^{-2})		
	Measured	Simulated	%Error	Measured	Simulated	%Error
1.21 m s^{-1}	1.483	1.349	9.04	1.674	1.832	9.44
1.69 m s^{-1}	1.979	1.725	12.83	2.194	2.359	7.52
2.05 m s^{-1}	2.468	2.177	11.79	2.738	2.823	3.11
3.10 m s^{-1}	2.988	2.881	3.58	3.865	3.591	7.09

Table 3 – Experimental and predicted RMS acceleration of tractor under different field road conditions.

Field road conditions	driver seat (m s^{-2})			cabin (m s^{-2})		
	Measured	Simulated	%Error	Measured	Simulated	%Error
Rough standard road	2.745	2.834	3.24	2.421	2.582	6.65
Rice straw field	0.759	0.807	6.32	0.622	0.697	12.06
Paddy field	0.512	0.542	5.86	0.467	0.453	2.99
Field road condition	chassis (m/s^2)			implement (m/s^2)		
	Measured	Simulated	%Error	Measured	Simulated	%Error
Rough standard road	2.154	2.204	2.32	2.821	2.934	4.01
Rice straw field	0.496	0.585	17.94	0.953	0.891	6.51
Paddy field	0.425	0.375	11.76	0.548	0.593	8.21

(I) without cabin, front axle suspension and implement;
(II) with cabin suspension, without front axle suspension and implement;
(III) with cabin suspension and implement, without front axle suspension;
(IV) with cabin, front axle suspension and implement.

The corresponding RMS of the vibration responses of tractor system under different settings are shown and listed in Table 4. Furthermore, the effect of the front axle suspension and the implement on rollover limit of the wheeled tractor/implement system is studied (Fig. 18).

Figure 18 shows that there are three different situations that the first wheel will be lifted. In the zone I, two front wheels of the tractor system without front axle suspension will lift simultaneously, because of the large slope angles. For the tractor without front axle suspension, the maximum slope angle ($\beta = 58.31^0$) arises when the orientation is $\sigma = \pm 23^0$. As $\sigma < 31^0$, there is no warning for the driver when the two wheels get off the ground and the farm tractor overturns backwards. In the symmetric zones II and III, there exists the lifting of the wheel for low slope angle. The minimum slope angle ($\beta = 30^0$ and $.24.7^0$) for tractor with/without the implement (with front axle suspension) arises when the orientation angle is $\sigma = \pm 99^0$. Similarly, the minimum slope angle ($\beta = 27^0$ and 22.34^0) for tractor with/without the implement (without front axle suspension) is reached with the orientation angle of $\sigma = \pm 99^0$. The farm tractor equipped with a suspended front axle has a higher rollover limit than that without front axle suspension. The presence of the front axle suspension and implement improves this minimum slope angle, meanwhile, reduces the maximum slope angle.

As can be seen from Table 4, the axle hydro-pneumatic suspension increases the vertical, lateral and roll vibration acceleration of chassis, the vertical vibration accelerations transmitted to the driver's seat in the case (IV) also rise compared with those in the case without front axle hydro-

Table 4 – RMS of vibration responses of tractor system under different settings.

Settings	$\ddot{x}_b$ (m s^{-2})	$\ddot{y}_b$ (m s^{-2})	$\ddot{z}_b$ (m s^{-2})	$\ddot{z}_d$ (m s^{-2})	$\ddot{\varphi}_{b1}$ (rad s^{-2})	$\ddot{\varphi}_{b2}$ (rad s^{-2})	F_{fdyn} (N)	
Case I	2.243	0.193	1.935	2.131	1.353	0.932	2678.5 R	2648.1 L
Case II	1.723	0.179	1.647	1.932	1.519	0.616	2986.5 R	3264.9 L
Case III	1.626	0.158	1.331	1.535	1.351	0.986	5934.3 R	6289.8 L
Case IV	1.495	0.185	1.525	2.231	0.785	0.622	3314.6 R	3516.3 L

R-right tyre, L-left tyre.

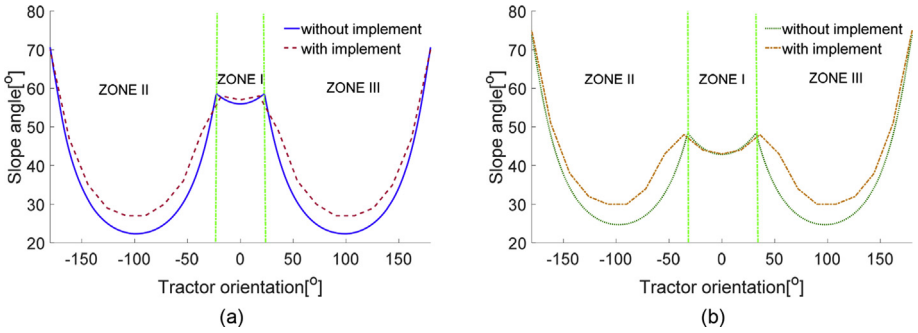


Fig. 18 – Rollover limits chart of tractor/implement system: (a) without front axle suspension, (b) with front axle suspension.

pneumatic suspension, whilst reducing the longitudinal, vertical, pitch vibration of chassis, the dynamic load on the two front tyres. The passive cabin suspension can significantly weaken the vertical vibration intensity of driver seat, cabin, chassis as well as the dynamic load of two front tyres compared with those in the case (I). In the case (III), the vertical vibrations of the driver's seat, longitudinal, lateral, vertical and pitch vibrations of chassis are much smaller than those in case (II), but the roll vibration of the chassis and the dynamic load of two front tyres increases significantly. Therefore, the front axle hydro-pneumatic suspension will deteriorate the ride comfort of the driver but improve the handing stability (pitch and roll stability) obviously. The passive cabin suspension plays a more important role in improving the ride comfort of the driver than the front axle hydro-pneumatic suspension does, while compromising the pitch stability to some extent. The existence of implement will raise the comfort of the driver and the pitch stability of a tractor, at the same time, drastically worsen the roll stability.

4.1. *Effect of nitrogen volume of accumulators*

In this section, the effect of initial nitrogen volume of the accumulators A and B is simulated. When the forward speed is 1.21 m/s and the nitrogen pressure of the accumulators A and B is 6 MPa, the RMS of the vibration responses of the tractor/implement system (the orifice diameter 2.4 mm of throttle valves 6 and 8, and 0 or 5 mm of throttle valve 9 for the front axle hydro-pneumatic suspension) under different initial nitrogen volumes of the accumulators A and B is recorded and listed in Table 5.

Table 5 shows that when the throttle valve 9 is closed, the longitudinal, lateral and vertical as well as roll vibration of chassis, the dynamic load of two front tyres increase at first and begin to decrease with the rise of the nitrogen volume of the accumulators A and B. The vertical vibration acceleration of driver increase, while the pitch vibration of the chassis decreases. When the throttle valve 9 is fully opened, the longitudinal acceleration of the chassis and the dynamic load of the two front tyres increase initially and begin to decrease with the increase in nitrogen volume of the accumulators A and B, while the lateral and roll acceleration of the chassis reduce at first and then rise. The vertical and pitch acceleration of the chassis decrease with the increase of nitrogen volume of the accumulators A and B. On the contrary, the vertical acceleration of driver seat increase. Generally, the RMS of the pitch vibration of the chassis and the dynamic load of two front tyres are more sensitive to the change of the initial nitrogen volume of the accumulators A and B, while the RMS of other tractor's vibration responses are insensitive to the change of the initial nitrogen volume of the accumulators and almost keep constant whether the throttle valve is closed or opened. For the purpose of improving the pitch stability of the tractor/implement system, the optimised initial nitrogen volume of the front axle hydro-pneumatic suspension should be 0.7 L.

Table 5 – RMS of tractor's vibration responses under different nitrogen volumes of accumulators.

Orifice diameter 0 mm of throttle valve 9 (closed)								
Nitrogen volume of accumulators	$\ddot{x}_b$(m s^{-2})	$\ddot{y}_b$(m s^{-2})	$\ddot{z}_b$(m s^{-2})	$\ddot{z}_d$(m s^{-2})	$\ddot{\varphi}_{b1}$(rad s^{-2})	$\ddot{\varphi}_{b2}$(rad s^{-2})	F_{fdyn}(N)	
0.3 L	1.4707	0.1716	1.5471	2.0647	1.1249	0.6624	3344.8 R	3237.3 L
0.4 L	1.4870	0.1789	1.5922	2.1050	1.1060	0.6681	3564.3 R	3327.3 L
0.5 L	1.4953	0.1850	1.6286	2.1347	1.0860	0.6716	3654.9 R	3409.3 L
0.6 L	1.4828	0.1841	1.4793	2.1550	0.9514	0.6715	3350.8 R	3251.3 L
0.7 L	1.4589	0.1775	1.4637	2.1632	0.9346	0.6673	3105.9 R	3177.9 L
Orifice diameter 5 mm of throttle valve 9 (fully opened)								
Nitrogen volume of accumulators	$\ddot{x}_b$(m s^{-2})	$\ddot{y}_b$(m s^{-2})	$\ddot{z}_b$(m s^{-2})	$\ddot{z}_d$(m s^{-2})	$\ddot{\varphi}_{b1}$(rad s^{-2})	$\ddot{\varphi}_{b2}$(rad s^{-2})	F_{fdyn}(N)	
0.3 L	1.7767	0.1875	1.5794	2.1513	1.2697	0.6725	2645.1 R	3061.6 L
0.4 L	1.7816	0.1819	1.5035	2.1714	1.0834	0.6696	3356.5 R	3386.7 L
0.5 L	1.8232	0.1760	1.4807	2.1763	0.9171	0.6664	3442.1 R	3996.7 L
0.6 L	1.7686	0.1818	1.4394	2.1957	0.8342	0.6682	2957.7 R	3475.2 L
0.7 L	1.6092	0.1849	1.4210	2.2028	0.7721	0.6723	2841.0 R	3110.2 L

4.2. *Effect of nitrogen pressure of accumulators*

When the forward speed of the tractor is 1.21 m/s, the initial nitrogen volumes of accumulators A and B is 0.5 L, the RMS of the vibration responses of the tractor/implement system with the orifice diameter 2.4 mm of throttle valves 6 and 8 of front axle hydro-pneumatic suspension under different nitrogen pressure of accumulators A and B is recorded and listed in Table 6.

Table 6 shows that when the throttle valve 9 is closed, the longitudinal and roll acceleration of chassis, vertical acceleration of driver and dynamic load of two front tyres decreases at first and then increases as the initial nitrogen pressure rises from 5.8 MPa to 6.2 MPa, they continue to decrease when the initial nitrogen pressure is above 6.2 MPa. The lateral, vertical and pitch accelerations of the chassis always reduced in the process. When the throttle valve 9 is fully opened, the longitudinal accelerations of the chassis increase at first and then decrease with the initial nitrogen pressure rising from 5.8 MPa to 6.2 MPa, and then rise again with the initial nitrogen pressure above 6.2 MPa. Meanwhile the dynamic load of two front tyres is changing reversely. The lateral and roll acceleration of chassis and the vertical acceleration of the driver rise with the increase in the initial nitrogen pressure of accumulators A and B, but the vertical and pitch acceleration of the chassis decrease. Therefore, the longitudinal and pitch acceleration of the chassis are sensitive to the change of the initial nitrogen pressure of accumulators A and B. The optimised initial nitrogen pressure for front axle hydro-pneumatic suspension is 6.5 MPa.

4.3. *Effect of orifice diameter of throttle valves 6 and 8*

The RMS of the vibration responses of the tractor/implement system (with the initial nitrogen volume 0.5 L of the accumulators A and B) under different orifice diameters of throttle valves 6 and 8 are listed in Table 7 for when the forward speed of the tractor was 1.21 m/s and the nitrogen pressure of the accumulators A and B is 6 MPa.

Table 7 shows that when the throttle valve 9 is closed, the longitudinal, vertical and pitch acceleration of chassis and the dynamic load of the two front tyres increase as the orifice diameter of throttle valves 6, 8 increases, while the lateral and roll acceleration of chassis and vertical acceleration of the driver increase at first and then decrease. When the throttle valve 9 is fully opened, the longitudinal, vertical and pitch acceleration of the chassis, vertical acceleration of driver and the dynamic load of two front tyres increase as the orifice diameter of the throttle valves 6, 8 increases, but the lateral and roll accelerations of the chassis reduce at first and then rise with the orifice diameter of throttle valves 6, 8 increasing from 1 mm to 4 mm. Therefore, the longitudinal and pitch acceleration of chassis are sensitive to the orifice diameter change of throttle valves 6, 8. The recommended orifice

Table 6 – RMS of tractor's vibration responses under different nitrogen pressure of accumulators.

Orifice diameter 0 mm of throttle valve 9 (closed)								
Nitrogen pressure of accumulators	$\ddot{x}_b$(m s^{-2})	$\ddot{y}_b$(m s^{-2})	$\ddot{z}_b$(m s^{-2})	$\ddot{z}_d$(m s^{-2})	$\ddot{\varphi}_{b1}$(rad s^{-2})	$\ddot{\varphi}_{b2}$(rad s^{-2})	F_{fdyn}(N)	
5.8 MPa	1.5006	0.1890	1.5580	2.1398	1.1521	0.6740	1455.8 R	5947.6 L
6.0 MPa	1.4953	0.1850	1.5405	2.1278	1.1103	0.6715	1391.7 R	5598.1 L
6.2 MPa	1.5788	0.1840	1.5286	2.1347	1.0860	0.6725	1354.9 R	5309.3 L
6.5 MPa	1.5272	0.1805	1.5248	2.1113	1.0522	0.6680	1314.4 R	4938.7 L
Orifice diameter 5 mm of throttle valve 9 (fully opened)								
Nitrogen pressure of accumulators	$\ddot{x}_b$(m s^{-2})	$\ddot{y}_b$(m s^{-2})	$\ddot{z}_b$(m s^{-2})	$\ddot{z}_d$(m s^{-2})	$\ddot{\varphi}_{b1}$(rad s^{-2})	$\ddot{\varphi}_{b2}$(rad s^{-2})	F_{fdyn}(N)	
5.8 MPa	1.7991	0.1754	1.5316	2.1724	1.0661	0.6658	1378.4 R	3441.6 L
6.0 MPa	1.8233	0.1760	1.5144	2.1749	0.9758	0.6664	1258.7 R	3203.1 L
6.2 MPa	1.7380	0.1791	1.4807	2.1761	0.9171	0.6665	1142.1 R	2996.7 L
6.5 MPa	1.7407	0.1908	1.4585	2.1846	0.9085	0.6759	1097.8 R	2845.2 L

Table 7 – RMS of tractor's vibration responses under different orifice diameters of throttle valves 6, 8.

Orifice diameter 0 mm of throttle valve 9 (closed)								
Orifice diameter of throttle valves 6, 8	$\ddot{x}_b$(m s^{-2})	$\ddot{y}_b$(m s^{-2})	$\ddot{z}_b$(m s^{-2})	$\ddot{z}_d$(m s^{-2})	$\ddot{\varphi}_{b1}$(rad s^{-2})	$\ddot{\varphi}_{b2}$(rad s^{-2})	F_{fdyn}(N)	
1 mm	0.7919	0.1771	1.4730	2.111	0.8991	0.6671	1077.3 R	3083.1 L
2 mm	0.9170	0.1895	1.4840	2.170	0.9384	0.6757	1136.7 R	3125.6 L
3 mm	1.1347	0.1902	1.5033	2.185	1.0012	0.6782	1231.1 R	3199.7 L
4 mm	1.5788	0.1840	1.5290	2.175	1.0861	0.6725	1354.9 R	3309.3 L
Orifice diameter 5 mm of throttle valve 9 (fully opened)								
Orifice diameter of throttle valves 6, 8	$\ddot{x}_b$(m s^{-2})	$\ddot{y}_b$(m s^{-2})	$\ddot{z}_b$(m s^{-2})	$\ddot{z}_d$(m s^{-2})	$\ddot{\varphi}_{b1}$(rad s^{-2})	$\ddot{\varphi}_{b2}$(rad s^{-2})	F_{fdyn}(N)	
1 mm	0.8722	0.1845	1.4370	2.1642	0.8066	0.6717	934.3 R	2862.3 L
2 mm	1.0357	0.1804	1.4470	2.1671	0.8301	0.6711	982.9 R	2891.6 L
3 mm	1.4197	0.1734	1.4626	2.1724	0.8701	0.6641	1055.7 R	2937.8 L
4 mm	1.8232	0.1760	1.4807	2.1762	0.9171	0.6664	1142.1 R	2996.7 L

diameter of the throttle valves 6 and 8 is 1 mm to obtain a better ride comfort and handling stability.

5. Conclusion

A complete three dimensional dynamic model of the wheeled tractor/implement system with a front axle hydro-pneumatic suspension is established. The model considers the effect of implement, rubber cabin suspension and front axle hydro-pneumatic suspension together. The predictive vibration characteristics of the proposed model agree with the measured results very well and the model is validated. A comparative study on the effect of the passive cabin suspension, the implement and the front axle hydro-pneumatic suspension on the vibration characteristics of tractor system under four cases is made. The simulation results show that the front axle hydro-pneumatic suspension will deteriorate the ride comfort but improve the pitch and roll stability. The passive cabin suspension plays a more important role in improving the ride comfort than the front axle hydro-pneumatic suspension does, while taking the expense of pitch stability in some degree. Using an implement will raise the comfort of the driver and improve the pitch stability of tractor, but dramatically worsen the roll stability. The front axle suspension and the use of the implement improve the minimum slope angle and reduce the maximum slope angle.

The optimised initial nitrogen volume and pressure for improving the pitch stability of the wheeled tractor/implement system with front axle hydro-pneumatic suspension is 0.7 L and 6.5 MPa. The RMS of the pitch vibration of chassis and dynamic load of two front tyres are more sensitive to the change of the initial nitrogen volume of accumulators, while the longitudinal and pitch acceleration of the chassis are sensitive to the change of the initial nitrogen pressure of the accumulators and the orifice diameter of throttle valves. The recommended orifice diameter of the throttle valves for obtaining better ride comfort and handling stability is 1 mm.

Three dimensional dynamic model of the wheeled tractor/implement system with front axle hydro-pneumatic suspension under ploughing conditions considering the effect of thrust, guide bars and optimum control of front axle hydro-pneumatic suspension will be pursued in future research to reach a good balance between the ride comfort and the handing stability of tractor system.

Acknowledgements

This paper has been partially supported by the two research projects: “China Postdoctoral Fund”, Grant #2016M591855 and “National Natural Science Foundation of China”, Grant #51275249.

Appendix A. Supplementary data

Supplementary data to this article can be found online at https://doi.org/10.1016/j.biosystemseng.2019.05.004.

REFERENCES

Adam, S. A., & Jalil, N. A. A. (2017). Vertical suspension seat transmissibility and seat values for seated person exposed to whole-body vibration in agricultural tractor preliminary study. *Procedia Engineering, 170*, 435–442.

Ahmed, O. B., & Goupillon, J. F. (1997). Predicting the ride vibration of an agricultural tractor. *Journal of Terramechanics, 34*(1), 1–11.

Arvidsson, J., & Ristic, S. (1996). Soil stress and compaction effects for four tractor tyres. *Journal of Terramechanics, 33*(5), 223–232.

Clijmans, L., Ramon, H., & De Baerdemaeker, J. (1998). Structural modification effects on the dynamic behavior of an agricultural tractor. *Transactions of the ASAE, 41*(1), 5–10.

Crolla, D. A., Horton, D. N. L., & Stayner, R. M. (1990). Effect of tyre modelling on tractor ride vibration predictions. *Journal of Agricultural Engineering Research, 47*, 55–77.

Cuong, D. M., Zhu, S. H., & Ngoc, N. T. (2014). Study on the variation characteristics of vertical equivalent damping ratio of tire–soil system using semi-empirical model. *Journal of Terramechanics, 51*, 67–80.

Cuong, D. M., Zhu, S. H., & Zhu, Y. (2013). Effects of tyre inflation pressure and forward speed on vibration of an unsuspended tractor. *Journal of Terramechanics, 50*(3), 185–198.

Cutini, M., Costa, C., & Bisaglia, C. (2016). Development of a simplified method for evaluating agricultural tractor's operator whole body vibration. *Journal of Terramechanics, 63*, 23–32.

De Temmerman, J., Deprez, K., Anthonis, J., & Ramon, H. (2004). Conceptual cab suspension system for a self-propelled agricultural machine, Part 1: Development of a linear mathematical model. *Biosystems Engineering, 89*(4), 409–416.

Deprez, K., Moshou, D., Anthonis, J., Baerdemaeker, J. D., & Ramon, H. (2005). Improvement of vibrational comfort by passive and semi-active cabin suspensions. *Computers and Electronics in Agriculture, 49*, 431–440.

Gobbi, M., Mastinu, G., & Previati, G. (2014). Farm tractors with suspended front axle: Anti-dive and anti-lift characteristics. *Journal of Terramechanics, 56*, 157–172.

Hammond, J. K., & Harrison, R. F. (1981). Nonstationary response of vehicles on rough ground-a state space approach. *Journal of Dynamic Systems Measurement and Control, 103*(3), 245–250.

Hildebrand, R., Keskinen, E., & Navarrete, J. A. R. (2008). Vehicle vibrating on a soft compacting soil half-space: Ground vibrations, terrain damage, and vehicle vibrations. *Journal of Terramechanics, 45*(4), 121–136.

Kumar, A., Mahajan, P., Mohan, D., & Varghese, M. (2001). IT-information technology and the human interface: Tractor vibration severity and driver health: A study from rural India. *Journal of Agricultural Engineering Research, 80*(4), 313–328.

Lehtonen, T. J., & Juhala, M. (2005). Predicting the ride behaviour of a suspended agricultural tractor. *International Journal of Vehicle Systems Modelling and Testing, 1*(1–3), 131–142.

Li, Z., Mitsuoka, M., Inoue, E., Okayasu, T., & Hirai, Y. (2015). Development of stability indicators for dynamic Phase I overturn of conventional farm tractors with front axle pivot. *Biosystems Engineering, 134*, 55–67.

Lines, J. A., & Murphy, K. (1991a). The stiffness of agricultural tractor tyres. *Journal of Terramechanics, 28*(1), 49–64.

Lines, J. A., & Murphy, K. (1991b). The radial damping of agricultural tractor tyres. *Journal of Terramechanics, 28*(2–3), 229–241.

Lines, J. A., Stiles, M., & Whyte, R. (1995). Whole body vibration during tractor driving. *Journal of Low Frequency Noise Vibration and Active Control, 14*(2), 87–104.

Marsili, A., Ragni, L., Santoro, G., Servadio, P., & Vassalini, G. (2002). PM-power and machinery: Innovative systems to reduce vibrations on agricultural tractors: Comparative

analysis of acceleration transmitted through the driving seat. *Biosystems Engineering, 81*(1), 35–47.
Martelli, M., Paoluzzi, R., & Zarotti, L. G. (2002). The front suspension of agricultural tractors. In *14th International Conference of the International Society for Terrain-Vehicle Systems, Vicksburg, USA* (pp. 20–24).
Mazhei, A. A., Uspenskiy, A. A., & Ermalenok, V. G. (2006). *Dynamic analysis of the hydro-pneumatic front axle suspension of agriculture tractor*. SAE Technical Paper (pp. 1–6).
Melzi, S., Negrini, S., & Sabbioni, E. (2014). Numerical analysis of the effect of tire characteristics, soil response and suspensions tuning on the comfort of an agricultural vehicle. *Journal of Terramechanics, 55*, 17–27.
Muzammil, M., Siddiqui, S. S., & Hasan, F. (2004). Physiological effect of vibrations on tractor drivers under variable ploughing conditions. *Journal of Occupational Health, 46*(5), 403–409.
Nguyen, V. N., & Inaba, S. (2011). Effects of tire inflation pressure and tractor velocity on dynamic wheel load and rear axle vibrations. *Journal of Terramechanics, 48*(1), 3–16.
Prasad, N., Tewari, V. K., & Yadav, R. (1995). Tractor ride vibration-A review. *Journal of Terramechanics, 32*(4), 205–219.
Previati, G., Gobbi, M., & Mastinu, G. (2014). Mathematical models for farm tractor rollover prediction. *International Journal of Vehicle Design, 64*(2–4), 280–303.
Rabbani, M. A., Tsujimoto, T., Mitsuoka, M., Inoue, E., & Okayasu, T. (2011). Prediction of the vibration characteristics of half-track tractor considering a three-dimensional dynamic model. *Biosystems Engineering, 110*(2), 178–188.
Rehnberg, A. (2011). *Suspension design for off-road construction machines*. Stockholm: KTH Royal Institute of Technology (Chapter 1).
Scarlett, A. J., Price, J. S., & Stayner, R. M. (2007). Whole-body vibration: Evaluation of emission and exposure levels arising from agricultural tractors. *Journal of Terramechanics, 44*(1), 65–73.
Shahgoli, G., Fielke, J., Saunders, C., & Desbiolles, J. (2010). Simulation of the dynamic behaviour of a tractor-oscillating subsoiler system. *Biosystems Engineering, 106*(2), 147–155.
Sim, K., Lee, H., Yoon, J. W., Choi, C., & Hwang, S. H. (2017). Effectiveness evaluation of hydro-pneumatic and semi-active cab suspension for the improvement of ride comfort of agricultural tractors. *Journal of Terramechanics, 69*, 23–32.
Theron, N. J., & Els, P. S. (2007). Modelling of a semi-active hydro-pneumatic spring damper unit. *International Journal of Vehicle Design, 45*(4), 501–521.
van der Westhuizen, S. F., & Els, P. S. (2015). Comparison of different gas models to calculate the spring force of a hydro-pneumatic suspension. *Journal of Terramechanics, 57*, 41–59.
Yang, Y., Ren, W. Q., Chen, L. P., Jiang, M., & Yang, Y. L. (2009). Study on ride comfort of tractor with tandem suspension based on multi-body system dynamics. *Applied Mathematical Modelling, 33*(1), 11–33.
Yilidaer, Y., Zhu, S. H., Xu, G., & Yuan, J. Q. (2015). Front axle suspension parameters match and its impact on vibration characteristics of tractor. *Transactions of the Chinese Society of Agricultural Engineering, 31*(10), 29–36.
Yin, Y., Rakheja, S., Yang, J., & Boileau, P. E. (2018). Characterization of a hydro-pneumatic suspension strut with gas-oil emulsion. *Mechanical Systems and Signal Processing, 106*, 319–333.
Yuan, J. Q., Zhu, S. H., Gao, Q., Xu, G., Ma, J. F., & Lu, Z. X. (2017). Design and characteristic study of tractor front axle hydro-pneumatic spring. *Journal of Nanjing Agricultural University, 40*(1), 176–185.
Zehsaz, M., Sadeghi, M. H., Ettefagh, M. M., & Shams, F. (2011). Tractor cabin's passive suspension parameters optimization via experimental and numerical methods. *Journal of Terramechanics, 48*(6), 439–450.
Zheng, E. L., Fan, Y. D., Zhu, R., Zhu, Y., & Xian, J. Y. (2016). Prediction of the vibration characteristics for wheeled tractor with suspended driver seat including air spring and MR damper. *Journal of Mechanical Science and Technology, 30*(9), 4143–4156.
Zhu, S. H., Xu, G., Yuan, J. Q., Ma, J. F., & Yilidaer, Y. (2014). Influence of implement's mass on vibration characteristics of tractor-implement system. *Transactions of the Chinese Society of Agricultural Engineering, 30*(24), 30–37.
Zhu, S. H., Zwiebel, S., & Bernhardt, G. (1999). A theoretical formula for calculating damping in the impact of two bodies in a multibody system. *Proceedings of the Institution of Mechanical Engineers Part C Journal of Mechanical Engineering Science, 213*(3), 211–216.